Viscoelastically coupled mechanics of fluid-conveying microtubes

Mergen H. Ghayesh [a,*], Ali Farajpour [a], Hamed Farokhi [b]

[a] *School of Mechanical Engineering, University of Adelaide, South Australia 5005, Australia*
[b] *Department of Mechanical and Construction Engineering, Northumbria University, Newcastle upon Tyne NE1 8ST, UK*
[*] *Corresponding author: mergen.ghayesh@adelaide.edu.au*

Abstract

In this paper, the complex viscoelastically coupled mechanics of fluid-conveying microtubes is examined for the first time. The externally excited microtube is assumed to be embedded in a nonlinear elastic medium. A scale-dependent theoretical model is developed with consideration of curvature nonlinearity within the context of the modified version of the couple stress theory (CST). According to Hamilton's energy/work principle, the coupled nonlinear equations of fluid-conveying microscale tubes are derived. Both the transverse and longitudinal displacements and inertia are taken into account in the continuum-based model and numerical calculations. In order to discretise the governing nonlinear differential equations, Galerkin's weighted-residual procedure is employed. The bifurcation characteristics of the fluid-conveying microsystem with clamped-clamped boundary conditions are obtained within the framework of a direct time-integration procedure. It is found that the complex dynamics of the fluid-conveying microsystem is very sensitive to the speed of the flowing fluid.

Keywords: Mechanics; Viscoelastic; Fluid-conveying microtubes; Nonlinearity; Size-dependent

1. Introduction

Microstructures/nanostructures [1-3] conveying fluid have lately been in the limelight of many researchers and scientists due to their fascinating applications in various fields of microtechnology. Some interesting practical uses of these microscale structures are briefly reviewed in the following. Alveringh et al. [4] showed that the transverse deformation of non-ideal microchannels with an imperfect circular cross-section can be used for pressure sensing. Another significant application of fluid-conveying microstructures is in biotechnology and modern medicine. More recently, Warkiani et al. [5] designed and fabricated a spiral microfluidic machine for isolation of tumour cells from the blood which is used for cancer diagnosis.

In order to accurately design and fabricate a microsystem/nanosystem [6-17], it is essential to increase the level of knowledge of its mechanical behaviour including its deformation under different applied mechanical forces, especially in the presence of ultrasmall size effects [18-28]. To this end, the development of theoretical continuum-based models is very useful to pave the way for the formulation of experimental observations [29-34]. The application of the classical scale-free elasticity to these structures may be inaccurate since the mechanical properties of micro/nanoscale structures have been proved to be size-dependent [35-42]. During the last decade, some scale-dependent elasticity theories [43, 44] such as the modified couple stress (MCS), the strain gradient elasticity (SGE), the nonlocal continuum mechanics (NCM) and the nonlocal strain gradient (NSGT) were introduced. All these modified continuum-based theories contain at least one small scale parameter which makes them capable of predicting size effects. In comparison with the molecular dynamics (MD) simulation

and experimental techniques which are difficult to implement at small scales, the simplicity and convenience of scale-dependent continuum models have increased their popularity in recent years. While the NCM has been widely employed for nanomaterials such as carbon nanotubes, graphene sheets, and piezoelectric nanofilms [45], the MCS theory has been mainly utilised to investigate the mechanical response of microplates [46] and microbeams [47]. For this reason, in the present analysis the modified version of the couple stress elasticity is employed.

A vast number of investigations has been reported on the mechanics of *macro*structures conveying fluid; only a few number of them is reviewed here. The influence of a transverse spring support on the stability of macroscale pipes carrying flowing fluid was investigated by Sugiyama et al. [48]. Ghayesh et al. [49] also developed a three-dimensional theoretical model to examine the dynamic response of fluid-conveying cantilevered macroscale pipes with an attached mass at the tip and an intermediate spring support. Furthermore, they conducted some experiments to evaluate and calibrate the proposed continuum model.

In addition to the development of continuum models for macrostructures containing flowing fluid, in a few recent years, some size-dependent theoretical models have been invented to explore the statics and dynamics of *micro/nano scale* structures conveying fluid. Wang [50] developed a higher-order scale-dependent mathematical model in order to study the vibrational response of fluid-conveying microtubes; in order to capture the size effects, he incorporated one length-scale coefficient into a mathematical model based on the MCS theory. It was observed that as the velocity of the internal flow increases, the fundamental frequencies of the microsystem decrease. In another article, Kural and Özkaya [51] examined the vibration

behaviour of a fluid-conveying microscale beam on an elastic bed using the modified version of the MCS theory together with a multiple timescale technique as a solution approach for the differential equations of motion. Dehrouyeh-Semnani et al. [52] presented a nonlinear continuum-based model to analyse the flow-induced dynamic response of both macroscale and microscale pipes carrying flowing fluid in pre- and post-flutter regimes employing the MCS theory; they used the Runge–Kutta method and the Galerkin approach so as to solve the nonlinear differential equations of motion. In addition, a stability analysis was reported in Ref. [53] on the fluid-conveying microscale pipes with fixed-free boundary conditions. Mohammadimehr and Mehrabi [54] also studied the stability and frequency responses of double-bonded axisymmetric cylindrical microshells conveying fluid via the MCS Reddy shells theory as well as the generalised differential quadrature method. More recently, the large amplitude free and forced vibration analyses of fluid-conveying micropipes [18], carbon nanotubes and piezoelectric nanotubes have been reported, showing that the mechanical behaviour of these small-scale structures is highly size-dependent.

This work is aimed at analysing the scale-dependent viscoelastically coupled mechanics of fluid-conveying microtubes; this is for the first time. It is assumed that the microtube resting on an elastic foundation is subject to an external distributed dynamic loading as well. Using Hamilton's technique, the non-conventional coupled nonlinear differential equations, which govern the complex dynamics of the fluid-conveying microsystem, are derived. Both transverse and axial displacements are taken into account in the analysis. The discretised form of the governing equations are formulated applying the Galerkin procedure to the size-dependent continuum-based model of the microtube. The boundary conditions of the system are assumed

to be clamped at both ends. The resultant discretised equations are then solved with the help of a time-integration procedure. The influence of the fluid velocity on the bifurcation curves of Poincaré sections of fluid-conveying viscoelastic microtubes is studied in details. In addition, more details of the complex dynamics of the microsystem is given by plotting time histories and fast Fourier transforms (FFTs) as well as phase-plane portraits.

2. Scale-dependent continuum model and method of solution

Figure 1 depicts the schematic representation of a viscoelastic microtube that contains a flowing fluid and is embedded in a nonlinear elastic medium. Moreover, the microtube is assumed to be under the action of an external excitation load in the form of $F(x)\cos(\omega t)$. The flow speed, the length, the inner and outer diameters of the micropipe are shown by U_f, L, D_i, and D, respectively. It is assumed that the fluid speed is neither a function of time nor a function of the Cartesian coordinates (x,z). Both axial and transverse oscillations are taken into consideration in the present study.

In the present section, first the scale-dependent governing differential equations of the fluid-conveying microtube are derived with consideration of different sources of nonlinearity in order to explore the global complex dynamic behaviour of this microsystem. Then, the derived differential equations are discretised with the help of Galerkin procedure. Finally, the complex fluid-structure bifurcations of the fluid-conveying microscale system are obtained and analysed.

Applying the nonlinear Euler-Bernoulli beam (EBB) model, the axial strain of the microscale pipe (ε_{xx}) can be expressed as

$$\varepsilon_{xx}(x,z,t)=-z\left[\frac{\partial\theta(x,t)}{\partial x}\right]+\left\{\left[\left(\frac{\partial\hat{w}(x,t)}{\partial x}\right)^2+\left(\frac{\partial\hat{u}(x,t)}{\partial x}+1\right)^2\right]^{\frac{1}{2}}-1\right\}, \tag{1}$$

where $\hat{u}$, $\hat{w}$ and θ stand for the centreline axial displacement, transverse displacement and rotation, respectively.

To capture the size dependence of the system higher-order strains and stresses based on the modified couple stress theory are defined, i.e. the symmetric curvature (SCU) tensor, and the deviatoric part of the symmetric couple stress (SCS) tensor, denoted by $\boldsymbol{\chi}$ and $\boldsymbol{m}$, respectively. The non-zero components of the SCU tensor (χ_{ij}) are obtained as

$$\chi_{xy}=\frac{1}{4}\left\{z\left(\cos\theta\left(\frac{\partial\theta}{\partial x}\right)^2+\sin\theta\frac{\partial^2\theta}{\partial x^2}\right)-\frac{\partial\theta}{\partial x}\cos\theta-\frac{\partial^2\hat{w}}{\partial x^2}\right\},\qquad \chi_{yz}=\frac{\sin\theta}{4}\frac{\partial\theta}{\partial x}. \tag{2}$$

Regarding the Kelvin-Voigt model of viscoelasticity, the axial stress, σ_{xx}, and the components of the deviatoric part of the SCS, in general, are given by

$$\begin{aligned}&\sigma_{xx}=\sigma_e+\sigma_v,\quad \langle\sigma_e,\sigma_v\rangle=\left\langle E\varepsilon_{xx},\alpha\frac{\partial\varepsilon_{xx}}{\partial t}\right\rangle.\\ &m_{ij}=m_{ij(e)}+m_{ij(v)},\quad \langle m_{ij(e)},m_{ij(v)}\rangle=\left\langle\frac{l^2E}{1+\nu},\frac{l^2\alpha}{1+\nu}\right\rangle\chi_{ij},\end{aligned} \tag{3}$$

where [α, E] represent the viscosity coefficient and Young's modulus, respectively, l stands for the length-scale parameter of the fluid-conveying microsystem; the subscripts *e* and *v* denote the elastic and viscoelastic parts, respectively.

The motion energy variation of the microsystem is given by

$$\begin{aligned}\delta K = & M\int_0^L\left(\frac{\partial \hat{w}}{\partial t}+U_f\frac{\partial \hat{w}}{\partial X}\right)\delta\left(\frac{\partial \hat{w}}{\partial t}+U_f\frac{\partial \hat{w}}{\partial X}\right)\mathrm{d}x + m\int_0^L\frac{\partial \hat{u}}{\partial t}\delta\frac{\partial \hat{u}}{\partial t}\mathrm{d}x \\ & + M\int_0^L\left[\frac{\partial \hat{u}}{\partial t}+\left(1+\frac{\partial \hat{u}}{\partial x}\right)U_f\right]\delta\left[\frac{\partial \hat{u}}{\partial t}+\left(1+\frac{\partial \hat{u}}{\partial x}\right)U_f\right]\mathrm{d}x + m\int_0^L\frac{\partial \hat{w}}{\partial t}\delta\frac{\partial \hat{w}}{\partial t}\mathrm{d}x,\end{aligned} \tag{4}$$

where *m* and *M* are respectively the mass per unit length of the microtube and the fluid. Furthermore, one can obtain the elastic energy variation induced by the surrounding elastic medium as

$$\delta U_s = \int_0^L\left(k_1\hat{w}+k_2\hat{w}^3\right)\delta\hat{w}\,\mathrm{d}x, \tag{5}$$

in which k_1 and k_2 are respectively the linear and nonlinear elastic coefficients of the surrounding medium. Taking into account the strain energy, non-conservative work of viscous stress, and work of external load, and utilising generalised Hamilton's principle, one can obtain the following nonlinear scale-dependent model for the fluid-conveying microscale tube with an internal dissipation (in which nonlinear terms up to third-order are retained)

$$
\begin{aligned}
&\left(m+M\right)\frac{\partial^2\hat{u}}{\partial t^2}+\left(MU_f^2-EA\right)\frac{\partial^2\hat{u}}{\partial x^2}+2MU_f\frac{\partial^2\hat{u}}{\partial x\partial t}-\alpha A\frac{\partial^3\hat{u}}{\partial t\partial x^2}\\
&-EA\frac{\partial\hat{w}}{\partial x}\frac{\partial^2\hat{w}}{\partial x^2}-\left(EI+\frac{1}{2}\mu Al^2\right)\left(\frac{\partial^2\hat{w}}{\partial x^2}\frac{\partial^3\hat{w}}{\partial x^3}+\frac{\partial\hat{w}}{\partial x}\frac{\partial^4\hat{w}}{\partial x^4}\right)\\
&-\alpha\left\{A\left(\frac{\partial^2\hat{w}}{\partial t\partial x}\left(\frac{\partial^2\hat{w}}{\partial x^2}\right)+\left(\frac{\partial^3\hat{w}}{\partial t\partial x^2}\right)\frac{\partial\hat{w}}{\partial x}\right)+\left[I+\frac{Al^2}{4\left(1+\nu\right)}\right]\left(\left(\frac{\partial^2\hat{w}}{\partial x^2}\right)\frac{\partial^4\hat{w}}{\partial t\partial x^3}+\frac{\partial\hat{w}}{\partial x}\left(\frac{\partial^5\hat{w}}{\partial t\partial x^4}\right)\right)\right\}=0,
\end{aligned}
\tag{6}
$$

$$
\begin{aligned}
&\left(m+M\right)\frac{\partial^2\hat{w}}{\partial t^2}+\left(MU_f^2-T\right)\frac{\partial^2\hat{w}}{\partial x^2}+2MU_f\frac{\partial^2\hat{w}}{\partial x\partial t}-f_1\cos\left(\omega t\right)\\
&-EA\left[\frac{3}{2}\left(\frac{\partial\hat{w}}{\partial x}\right)^2\left(\frac{\partial^2\hat{w}}{\partial x^2}\right)+\left(\frac{\partial\hat{w}}{\partial x}\right)\frac{\partial^2\hat{u}}{\partial x^2}+\frac{\partial^2\hat{w}}{\partial x^2}\left(\frac{\partial\hat{u}}{\partial x}\right)\right]+EI\frac{\partial^4\hat{w}}{\partial x^4}\\
&-EI\left[2\left(\frac{\partial^2\hat{w}}{\partial x^2}\right)^3+3\left(\frac{\partial^2\hat{w}}{\partial x^2}\right)\left(\frac{\partial^3\hat{u}}{\partial x^3}\right)+2\left(\frac{\partial^4\hat{w}}{\partial x^4}\right)\left(\frac{\partial\hat{w}}{\partial x}\right)^2+8\frac{\partial\hat{w}}{\partial x}\left(\frac{\partial^2\hat{w}}{\partial x^2}\right)\frac{\partial^3\hat{w}}{\partial x^3}+\left(\frac{\partial^4\hat{u}}{\partial x^4}\right)\frac{\partial\hat{w}}{\partial x}+2\frac{\partial\hat{u}}{\partial x}\frac{\partial^4\hat{w}}{\partial x^4}+4\frac{\partial^2\hat{u}}{\partial x^2}\frac{\partial^3\hat{w}}{\partial x^3}\right]\\
&-\frac{1}{4}\mu Il^2\left[3\frac{\partial^2\hat{w}}{\partial x^2}\left(\frac{\partial^3\hat{w}}{\partial x^3}\right)^2+6\frac{\partial\hat{w}}{\partial x}\frac{\partial^2\hat{w}}{\partial x^2}\frac{\partial^5\hat{w}}{\partial x^5}+10\frac{\partial\hat{w}}{\partial x}\frac{\partial^3\hat{w}}{\partial x^3}\frac{\partial^4\hat{w}}{\partial x^4}+\left(\frac{\partial\hat{w}}{\partial x}\right)^2\frac{\partial^6\hat{w}}{\partial x^6}+4\left(\frac{\partial^2\hat{w}}{\partial x^2}\right)^2\frac{\partial^4\hat{w}}{\partial x^4}\right]\\
&+\frac{1}{4}\mu Al^2\left[4\frac{\partial^4\hat{w}}{\partial x^4}-5\left(\frac{\partial^2\hat{w}}{\partial x^2}\right)^3-20\frac{\partial\hat{w}}{\partial x}\frac{\partial^2\hat{w}}{\partial x^2}\frac{\partial^3\hat{w}}{\partial x^3}-5\left(\frac{\partial\hat{w}}{\partial x}\right)^2\frac{\partial^4\hat{w}}{\partial x^4}\right.\\
&\qquad\left.-2\frac{\partial^4\hat{u}}{\partial x^4}\frac{\partial\hat{w}}{\partial x}-8\frac{\partial^2\hat{u}}{\partial x^2}\frac{\partial^3\hat{w}}{\partial x^3}-6\frac{\partial^3\hat{u}}{\partial x^3}\frac{\partial^2\hat{w}}{\partial x^2}-4\frac{\partial\hat{u}}{\partial x}\frac{\partial^4\hat{w}}{\partial x^4}\right]+k_1\hat{w}+k_2\hat{w}^3\\
&-\alpha A\left[2\frac{\partial^2\hat{w}}{\partial x^2}\frac{\partial^2\hat{w}}{\partial t\partial x}\frac{\partial\hat{w}}{\partial x}+\frac{\partial^3\hat{w}}{\partial t\partial x^2}\left(\frac{\partial\hat{w}}{\partial x}\right)^2+\frac{\partial\hat{w}}{\partial x}\frac{\partial^3\hat{u}}{\partial t\partial x^2}+\frac{\partial^2\hat{w}}{\partial x^2}\frac{\partial^2\hat{u}}{\partial t\partial x}\right]\\
&+\alpha I\left[\frac{\partial^5\hat{w}}{\partial t\partial x^4}-\frac{\partial^2\hat{w}}{\partial t\partial x}\frac{\partial^4\hat{u}}{\partial x^4}-\left(\frac{\partial^5\hat{u}}{\partial t\partial x^4}\right)\frac{\partial\hat{w}}{\partial x}-\left(\frac{\partial^2\hat{u}}{\partial x\partial t}\right)\frac{\partial^4\hat{w}}{\partial x^4}-2\frac{\partial\hat{u}}{\partial x}\frac{\partial^5\hat{w}}{\partial t\partial x^4}-3\left(\frac{\partial^4\hat{u}}{\partial t\partial x^3}\right)\frac{\partial^2\hat{w}}{\partial x^2}\right.\\
&\qquad-6\frac{\partial^2\hat{w}}{\partial t\partial x}\frac{\partial^3\hat{w}}{\partial x^3}\frac{\partial^2\hat{w}}{\partial x^2}-3\frac{\partial^3\hat{u}}{\partial t\partial x^2}\frac{\partial^3\hat{w}}{\partial x^3}-4\frac{\partial^4\hat{w}}{\partial t\partial x^3}\frac{\partial^2\hat{u}}{\partial x^2}-6\frac{\partial^3\hat{w}}{\partial t\partial x^2}\frac{\partial^3\hat{w}}{\partial x^3}\frac{\partial\hat{w}}{\partial x}-3\left(\frac{\partial^3\hat{w}}{\partial t\partial x^2}\right)\frac{\partial^3\hat{u}}{\partial x^3}\\
&\qquad\left.-6\frac{\partial^3\hat{w}}{\partial t\partial x^2}\left(\frac{\partial^2\hat{w}}{\partial x^2}\right)^2-2\left(\frac{\partial^5\hat{w}}{\partial t\partial x^4}\right)\left(\frac{\partial\hat{w}}{\partial x}\right)^2-8\frac{\partial^2\hat{w}}{\partial x^2}\frac{\partial\hat{w}}{\partial x}\left(\frac{\partial^4\hat{w}}{\partial t\partial x^3}\right)-2\frac{\partial\hat{w}}{\partial x}\frac{\partial^4\hat{w}}{\partial x^4}\frac{\partial^2\hat{w}}{\partial t\partial x}\right]
\end{aligned}
$$

$$
\begin{aligned}
&+\frac{\alpha A l^2}{8(1+\nu)}\Bigg[4\left(\frac{\partial^5\hat{w}}{\partial t\partial x^4}\right)-2\left(\frac{\partial^4\hat{u}}{\partial x^4}\right)\frac{\partial^2\hat{w}}{\partial t\partial x}-6\frac{\partial^4\hat{u}}{\partial t\partial x^3}\frac{\partial^2\hat{w}}{\partial x^2}-2\frac{\partial\hat{w}}{\partial x}\frac{\partial^5\hat{u}}{\partial t\partial x^4}-6\frac{\partial^3\hat{u}}{\partial x^3}\frac{\partial^3\hat{w}}{\partial t\partial x^2}-6\frac{\partial^3\hat{u}}{\partial t\partial x^2}\frac{\partial^3\hat{w}}{\partial x^3}\\
&\quad-2\frac{\partial^2\hat{u}}{\partial t\partial x}\frac{\partial^4\hat{w}}{\partial x^4}-4\frac{\partial^5\hat{w}}{\partial t\partial x^4}\frac{\partial\hat{u}}{\partial x}-8\frac{\partial^4\hat{w}}{\partial t\partial x^3}\frac{\partial^2\hat{u}}{\partial x^2}-15\frac{\partial^3\hat{w}}{\partial x^3}\frac{\partial\hat{w}}{\partial x}\frac{\partial^3\hat{w}}{\partial t\partial x^2}-17\frac{\partial^3\hat{w}}{\partial x^3}\frac{\partial^2\hat{w}}{\partial t\partial x}\frac{\partial^2\hat{w}}{\partial x^2}\\
&\quad-5\frac{\partial\hat{w}}{\partial x}\frac{\partial^2\hat{w}}{\partial t\partial x}\frac{\partial^4\hat{w}}{\partial x^4}-16\frac{\partial^3\hat{w}}{\partial t\partial x^2}\left(\frac{\partial^2\hat{w}}{\partial x^2}\right)^2-20\frac{\partial^4\hat{w}}{\partial t\partial x^3}\frac{\partial^2\hat{w}}{\partial x^2}\frac{\partial\hat{w}}{\partial x}-5\left(\frac{\partial\hat{w}}{\partial x}\right)^2\frac{\partial^5\hat{w}}{\partial t\partial x^4}\Bigg]\\
&-\frac{\alpha I l^2}{8(1+\nu)}\Bigg[\frac{\partial^2\hat{w}}{\partial t\partial x}\frac{\partial^2\hat{w}}{\partial x^2}\frac{\partial^5\hat{w}}{\partial x^5}+5\frac{\partial\hat{w}}{\partial x}\frac{\partial^3\hat{w}}{\partial t\partial x^2}\frac{\partial^5\hat{w}}{\partial x^5}+6\frac{\partial\hat{w}}{\partial x}\frac{\partial^2\hat{w}}{\partial x^2}\frac{\partial^6\hat{w}}{\partial t\partial x^5}+\left(\frac{\partial\hat{w}}{\partial x}\right)^2\frac{\partial^7\hat{w}}{\partial t\partial x^6}\\
&\quad+\frac{\partial\hat{w}}{\partial x}\frac{\partial^2\hat{w}}{\partial t\partial x}\frac{\partial^6\hat{w}}{\partial x^6}+6\frac{\partial^2\hat{w}}{\partial x^2}\frac{\partial^3\hat{w}}{\partial x^3}\frac{\partial^4\hat{w}}{\partial t\partial x^3}+4\frac{\partial^2\hat{w}}{\partial x^2}\frac{\partial^3\hat{w}}{\partial t\partial x^2}\frac{\partial^4\hat{w}}{\partial x^4}\\
&\quad+4\left(\frac{\partial^2\hat{w}}{\partial x^2}\right)^2\frac{\partial^5\hat{w}}{\partial t\partial x^4}+10\frac{\partial\hat{w}}{\partial x}\frac{\partial^4\hat{w}}{\partial t\partial x^3}\frac{\partial^4\hat{w}}{\partial x^4}+10\frac{\partial\hat{w}}{\partial x}\frac{\partial^3\hat{w}}{\partial x^3}\frac{\partial^5\hat{w}}{\partial t\partial x^4}\Bigg]=0.
\end{aligned}
\tag{7}
$$

In the above coupled equations f_1, μ, and T denote the transverse load, shear modulus, and axial pretension, respectively. In addition, it would be more convenient to rewrite Eqs. (6) and (7) in a dimensionless form; for this purpose, first the following dimension-free parameters are defined

$$
\begin{aligned}
&\bar{x}=\frac{\hat{x}}{L},\ \bar{u}=\frac{\hat{u}}{D},\ \bar{w}=\frac{\hat{w}}{D},\ S=\frac{L}{D},\ \tau=t\sqrt{\frac{EI}{L^4(M+m)}},\ \beta=\frac{M}{M+m},\\
&\alpha_v=\frac{\alpha}{E}\sqrt{\frac{EI}{(M+m)L^4}},\ \Pi_0=\frac{AL^2}{I},\ \Gamma=\frac{TL^2}{EI},\ \bar{\mu}=\frac{Al^2}{2(1+\nu)I},\\
&u_f=\sqrt{\frac{M}{EI}}U_f L,\ F_1=\frac{f_1L^4}{DEI},\ \Omega_e=\omega L^2\sqrt{\frac{M+m}{EI}},\ K_1=\frac{k_1L^4}{EI},\ K_2=\frac{k_2L^4D^2}{EI}.
\end{aligned}
\tag{8}
$$

Inserting the above parameters into Eqs. (6) and (7), the nonlinear scale-dependent model of the microscale system can be rewritten in non-dimensional forms.

The longitudinal displacement and transverse deflection of the viscoelastic microtube can be approximated as

$$\left\{\bar{w}(x,t)=\sum_{k=1}^{N_w} q_k(\tau)\bar{W}_k\right\};\quad \left\{\bar{u}(x,t)=\sum_{k=1}^{N_u} r_k(\tau)\bar{U}_k\right\}. \tag{9}$$

$\bar{W}_k$ and $\bar{U}_k$ are the shape functions; also, $q_k(\tau)$ and $r_k(\tau)$ stand for the *k*th transverse and axial generalised coordinates, respectively. Let us assume that the microtube is clamped at its both ends. Galerkin's decomposition approach to the resultant equations gives

$$\begin{aligned}
&\sum_{j=1}^{N_u}\left(\int_0^1 \bar{U}_i\bar{U}_j dx\right)\ddot{r}_j + 2\sqrt{\beta}u_f\sum_{j=1}^{N_u}\left(\int_0^1 \bar{U}_i\bar{U}_j' dx\right)\dot{r}_j + \left(u_f^2-\Pi_0\right)\sum_{j=1}^{N_u}\left(\int_0^1 \bar{U}_i\bar{U}_j'' dx\right)r_j \\
&-\frac{1}{S}\left(\frac{1}{2}\bar{\mu}+1\right)\sum_{j=1}^{N_w}\sum_{k=1}^{N_w}\left(\int_0^1 \bar{U}_i\bar{W}_j''\bar{W}_k''' dx+\int_0^1 \bar{U}_i\bar{W}_j'\bar{W}_k'''' dx\right)q_jq_k-\frac{\Pi_0}{S}\sum_{j=1}^{N_w}\sum_{k=1}^{N_w}\left(\int_0^1 \bar{U}_i\bar{W}_j'\bar{W}_k'' dx\right)q_jq_k \\
&-\Pi_0\alpha_v\sum_{j=1}^{N_u}\left(\int_0^1 \bar{U}_i\bar{U}_j'' dx\right)\dot{r}_j-\frac{\alpha_v(\Pi_0)}{S}\left\{\sum_{k=1}^{N_w}\sum_{j=1}^{N_w}\left(\int_0^1 \bar{U}_i\bar{W}_k'\bar{W}_j'' dx\right)\left(\dot{q}_kq_j+q_k\dot{q}_j\right)\right\} \\
&-\frac{\alpha_v}{S}\left(\frac{1}{2}\bar{\mu}+1\right)\sum_{j=1}^{N_w}\sum_{k=1}^{N_w}\left(\int_0^1 \bar{U}_i\bar{W}_j''\bar{W}_k''' dx+\int_0^1 \bar{U}_i\bar{W}_j'\bar{W}_k'''' dx\right)q_j\dot{q}_k=0, \qquad i=1,2,\ldots,N_u
\end{aligned} \tag{10}$$

$$\sum_{j=1}^{N_w}\left(\int_0^1 \bar{W}_i\bar{W}_j\,dx\right)\ddot{q}_j+2\sqrt{\beta}u_f\sum_{j=1}^{N_w}\left(\int_0^1 \bar{W}_i\bar{W}_j'dx\right)\dot{q}_j+u_f^2\sum_{j=1}^{N_w}\left(\int_0^1 \bar{W}_i\bar{W}_j''dx\right)q_j$$

$$+\left(1+\bar{\mu}\right)\sum_{j=1}^{N_w}\left(\int_0^1 \bar{W}_i\bar{W}_j''''dx\right)q_j+\alpha_v\left(1+\bar{\mu}\right)\sum_{j=1}^{N_w}\left(\int_0^1 \bar{W}_i\bar{W}_j''''dx\right)\dot{q}_j$$

$$-\Gamma\sum_{j=1}^{N_w}\left(\int_0^1 \bar{W}_i\bar{W}_j''dx\right)q_j-\frac{\Pi_0}{S}\left[\frac{1}{S}\frac{3}{2}\sum_{k=1}^{N_w}\sum_{j=1}^{N_w}\sum_{l=1}^{N_w}\left(\int_0^1 \bar{W}_i\bar{W}_k'\bar{W}_j'\bar{W}_l''dx\right)q_kq_jq_l\right.$$

$$\left.+\sum_{j=1}^{N_u}\sum_{k=1}^{N_w}\left(\int_0^1 \bar{W}_i\bar{U}_j''\bar{W}_k'\,dx+\int_0^1 \bar{W}_i\bar{U}_j'\bar{W}_k''dx\right)r_jq_k\right]$$

$$+K_1\sum_{j=1}^{N_w}\left(\int_0^1 \bar{W}_i\bar{W}_j\,dx\right)q_j+K_2\left\{\sum_{k=1}^{N_w}\sum_{j=1}^{N_w}\sum_{l=1}^{N_w}\left(\left(\int_0^1 \bar{W}_i\bar{W}_k\bar{W}_j\bar{W}_l\,dx\right)\right)q_kq_jq_l\right\}$$

$$-\frac{1}{S}\left[\sum_{k=1}^{N_u}\sum_{j=1}^{N_w}\left(3\int_0^1 \bar{W}_i\bar{U}_k'''\bar{W}_j''\,dx+\int_0^1 \bar{W}_i\bar{U}_k''''\bar{W}_j'dx+4\int_0^1 \bar{W}_i\bar{U}_k''\bar{W}_j'''dx+2\int_0^1 \bar{W}_i\bar{U}_k'\bar{W}_j''''dx\right)r_kq_j\right.$$

$$\left.+\frac{1}{S}\sum_{j=1}^{N_w}\sum_{k=1}^{N_w}\sum_{l=1}^{N_w}\left(2\int_0^1 \bar{W}_i\bar{W}_j''\bar{W}_k''\bar{W}_l''dx+2\int_0^1 \varphi_i\bar{W}_j'\bar{W}_k'\bar{W}_l''''dx+8\int_0^1 \bar{W}_i\bar{W}_j'\bar{W}_k''\bar{W}_l'''dx\right)q_jq_kq_l\right]$$

$$-\frac{\bar{\mu}}{4S}\left[\sum_{j=1}^{N_u}\sum_{k=1}^{N_w}\left(+6\left(\int_0^1 \bar{W}_i\bar{U}_j'''\bar{W}_k''\,dx\right)+8\int_0^1 \bar{W}_i\bar{U}_j''\bar{W}_k'''dx+2\left(\int_0^1 \bar{W}_i\bar{U}_j''''\bar{W}_k'dx\right)+4\int_0^1 \bar{W}_i\bar{U}_j'\bar{W}_k''''dx\right)r_jq_k\right.$$

$$\left.+\frac{1}{S}\sum_{j=1}^{N_w}\sum_{k=1}^{N_w}\sum_{l=1}^{N_w}\left(5\int_0^1 \bar{W}_i\bar{W}_j''\bar{W}_k''\bar{W}_l''dx+5\int_0^1 \bar{W}_i\bar{W}_j'\bar{W}_k'\bar{W}_l''''dx+20\int_0^1 \bar{W}_i\bar{W}_j'\bar{W}_k''\bar{W}_l'''dx\right)q_jq_kq_l\right]$$

$$-\frac{1}{4}\frac{\bar{\mu}}{\Pi_0S^2}\sum_{j=1}^{N_w}\sum_{k=1}^{N_w}\sum_{l=1}^{N_w}\left(3\int_0^1 \bar{W}_i\bar{W}_j''\bar{W}_k'''\bar{W}_l'''dx+6\int_0^1 \bar{W}_i\bar{W}_j'\bar{W}_k''\bar{W}_l^{(5)}dx+10\int_0^1 \bar{W}_i\bar{W}_j'\bar{W}_k'''\bar{W}_l''''dx\right.$$

$$\left.+\int_0^1 \bar{W}_i\bar{W}_j'\bar{W}_k'\bar{W}_l^{(6)}dx+4\int_0^1 \bar{W}_i\bar{W}_j''\bar{W}_k''\bar{W}_l''''dx\right)q_jq_kq_l$$

$$-\frac{\alpha_v\Pi_0}{S}\left[\frac{1}{S}\sum_{j=1}^{N_w}\sum_{k=1}^{N_w}\sum_{l=1}^{N_w}\left(\int_0^1 \bar{W}_i\bar{W}_j'\bar{W}_k'\bar{W}_l''dx\right)\left(2q_j\dot{q}_kq_l+q_jq_k\dot{q}_l\right)\right.$$

$$\left.+\sum_{j=1}^{N_u}\sum_{k=1}^{N_w}\left(\int_0^1 \bar{W}_i\bar{U}_j''\bar{W}_k'\,dx+\int_0^1 \bar{W}_i\bar{U}_j'\bar{W}_k''dx\right)\dot{r}_jq_k\right]$$

$$
\begin{aligned}
&-\frac{\alpha_v}{S}\Bigg[\sum_{k=1}^{N_u}\sum_{j=1}^{N_w}\left(3\int_0^1 \bar{W}_i\bar{U}_k'''\bar{W}_j''\,dx+\int_0^1 \bar{W}_i\bar{U}_k''''\bar{W}_j'\,dx\right)\left(\dot{r}_k q_j+r_k\dot{q}_j\right)\\
&\quad+\sum_{k=1}^{N_u}\sum_{j=1}^{N_w}\left(\int_0^1 \bar{W}_i\bar{U}_k''\bar{W}_j'''dx\right)\left(3\dot{r}_k q_j+4r_k\dot{q}_j\right)+\sum_{k=1}^{N_u}\sum_{j=1}^{N_w}\left(\int_0^1 \bar{W}_i\bar{U}_k'\bar{W}_j''''dx\right)\left(\dot{r}_k q_j+2r_k\dot{q}_j\right)\\
&\quad+\frac{1}{S}\sum_{j=1}^{N_w}\sum_{k=1}^{N_w}\sum_{l=1}^{N_w}\left(\int_0^1 \bar{W}_i\bar{W}_j'\bar{W}_k''\bar{W}_l'''dx\right)\left(6\dot{q}_j q_k q_l+6q_j\dot{q}_k q_l+8q_j q_k\dot{q}_l\right)\\
&\quad+\frac{2}{S}\sum_{j=1}^{N_w}\sum_{k=1}^{N_w}\sum_{l=1}^{N_w}\left(\int_0^1 \bar{W}_i\bar{W}_j'\bar{W}_k'\bar{W}_l''''dx\right)\left(\dot{q}_j q_k q_l+q_j q_k\dot{q}_l\right)+\frac{6}{S}\sum_{j=1}^{N_w}\sum_{k=1}^{N_w}\sum_{l=1}^{N_w}\left(\int_0^1 \bar{W}_i\bar{W}_j''\bar{W}_k''\bar{W}_l''dx\right)q_j q_k\dot{q}_l\Bigg]\\
&-\frac{\bar{\mu}\alpha_v}{4S}\sum_{j=1}^{N_u}\sum_{k=1}^{N_w}\left(6\int_0^1 \bar{W}_i\bar{U}_j'''\bar{W}_k''\,dx+2\int_0^1 \bar{W}_i\bar{U}_j''''\bar{W}_k'\,dx\right)\left(r_j\dot{q}_k+\dot{r}_j q_k\right)\\
&-\frac{\bar{\mu}\alpha_v}{4S}\sum_{j=1}^{N_u}\sum_{k=1}^{N_w}\left(\int_0^1 \bar{W}_i\bar{U}_j'\bar{W}_k''''dx\right)\left(4r_j\dot{q}_k+2\dot{r}_j q_k\right)-\frac{\bar{\mu}\alpha_v}{4S}\sum_{j=1}^{N_u}\sum_{k=1}^{N_w}\left(\int_0^1 \bar{W}_i\bar{U}_j''\bar{W}_k'''dx\right)\left(8r_j\dot{q}_k+6\dot{r}_j q_k\right)\\
&-\frac{\bar{\mu}\alpha_v}{4S^2}\sum_{j=1}^{N_w}\sum_{k=1}^{N_w}\sum_{l=1}^{N_w}\left(\int_0^1 \bar{W}_i\bar{W}_j'\bar{W}_k''\bar{W}_l'''dx\right)\left(17\dot{q}_j q_k q_l+15q_j\dot{q}_k q_l+20q_j q_k\dot{q}_l\right)\\
&-\frac{4\bar{\mu}\alpha_v}{S^2}\sum_{j=1}^{N_w}\sum_{k=1}^{N_w}\sum_{l=1}^{N_w}\left(\int_0^1 \bar{W}_i\bar{W}_j''\bar{W}_k''\bar{W}_l''dx\right)q_j q_k\dot{q}_l-\frac{5\bar{\mu}\alpha_v}{4S^2}\sum_{j=1}^{N_w}\sum_{k=1}^{N_w}\sum_{l=1}^{N_w}\left(\int_0^1 \bar{W}_i\bar{W}_j'\bar{W}_k'\bar{W}_l''''dx\right)\left(\dot{q}_j q_k q_l+q_j q_k\dot{q}_l\right)\\
&-\frac{\bar{\mu}\alpha_v}{4\Pi_0 S^2}\sum_{j=1}^{N_w}\sum_{k=1}^{N_w}\sum_{l=1}^{N_w}\left(\int_0^1 \bar{W}_i\bar{W}_j'\bar{W}_k''\bar{W}_l^{(5)}\,dx\right)\left(\dot{q}_j q_k q_l+6q_j q_k\dot{q}_l+5q_j\dot{q}_k q_l\right)\\
&-\frac{\bar{\mu}\alpha_v}{4\Pi_0 S^2}\sum_{j=1}^{N_w}\sum_{k=1}^{N_w}\sum_{l=1}^{N_w}\left(\int_0^1 \bar{W}_i\bar{W}_j'\bar{W}_k'\bar{W}_l^{(6)}\,dx\right)\left(q_j q_k\dot{q}_l+q_j\dot{q}_k q_l\right)-\frac{3\bar{\mu}\alpha_v}{2\Pi_0 S^2}\sum_{j=1}^{N_w}\sum_{k=1}^{N_w}\sum_{l=1}^{N_w}\left(\int_0^1 \bar{W}_i\bar{W}_j''\bar{W}_k'''\bar{W}_l'''dx\right)q_j q_k\dot{q}_l\\
&-\frac{5\bar{\mu}\alpha_v}{2\Pi_0 S^2}\sum_{j=1}^{N_w}\sum_{k=1}^{N_w}\sum_{l=1}^{N_w}\left(\int_0^1 \bar{W}_i\bar{W}_j'\bar{W}_k'''\bar{W}_l''''dx\right)\left(q_j q_k\dot{q}_l+q_j\dot{q}_k q_l\right)\\
&-\frac{\bar{\mu}\alpha_v}{\Pi_0 S^2}\sum_{j=1}^{N_w}\sum_{k=1}^{N_w}\sum_{l=1}^{N_w}\left(\int_0^1 \bar{W}_i\bar{W}_j''\bar{W}_k''\bar{W}_l''''dx\right)\left(q_j\dot{q}_k q_l+q_j q_k\dot{q}_l\right)=0, \qquad i=1,2,\ldots,N_w.
\end{aligned}
$$

(11)

Using Eqs. (10) and (11), one can construct a set of coupled nonlinear time-dependent differential equations so as to describe the complex bifurcation responses of fluid-conveying microtubes with an internal loss. In the present analysis, the number of shape functions along each axis is set to 10, leading to a discretised system with 20 degrees of freedom. Finally, with

the help of a backward differentiation formula (BDF) as a powerful numerical method, this nonlinear coupled system of equations are solved.

3. Numerical results for viscoelastically coupled mechanics

The complicated nonlinear viscoelastic behaviour of the fluid-conveying microscale system is investigated in the following in details by plotting the bifurcation curves associated with Poincaré sections. To obtain the numerical results, the elasticity modulus, E=1.44 GPa, ρ_p=1220 kg/m^3, and ν=0.38 are used. In addition, the density of the fluid is assumed to be equal to ρ_f =1000 kg/m^3 in the present analysis; D=55 μm, L/D = 100, and D_i=30 μm. Using these material and geometrical properties, the non-dimensional properties of the system are obtained as Π_0 =1.2331×10^5, β=0.2577, S=100, and $\overline{\mu}$ =0.4575. The dimensionless linear and nonlinear coefficients of the elastic bed are K_1=50.0 and K_2=50.0, respectively, while the remaining dimensionless parameters are taken as Γ =5.0, α_v=0.0002, and Ω_e/ω_1=1.0. Unless stated otherwise, these values are considered for the fluid-conveying microsystem throughout this section. It is worth mentioning that the critical flow velocity of the microscale pipe corresponding to divergence is obtained as 8.1446.

The bifurcation curves of Poincaré sections of fluid-conveying microscale pipes with viscoelastic properties are plotted in Fig. 2 for the generalised coordinates of motions along both directions; u_f =7.9 and ω_1=6.36. From Fig. 2a, it is found that the scale-dependent dynamic response consists of two main motion types: 1) period-1, and 2) period-3. Furthermore, no complicated motion such as chaos is observed in this figure. Complete details of the period-3

motion at F_1=18 is shown in Fig. 3. Time histories of q_1 and q_2 are plotted in Figs. 3a and 3b, respectively. In addition, the phase-plane portraits are depicted in Figs. 3c and 3d. Fast Fourier transforms (FFTs) of q_1 and q_2 are also illustrated in Figs. 3e and 3f, respectively, while their Poincaré sections are plotted in Figs. 3g and 3h.

The bifurcation diagrams of the fluid-conveying viscoelastic microsystem are indicated in Fig. 4 for u_f=8.1 which belongs to a microsystem within the subcritical region, but near the critical speed. An amount of 6.36 is obtained for the non-dimensional fundamental natural frequency of the system. It is observed that when the dimensionless speed of the flowing fluid increases from u_f=7.9 (Fig. 2) to u_f=8.1 (Fig. 4), the complex dynamic behaviour alters dramatically. The region in which the system motion is of period-1 type reduces while both diversity and complexity of the motion increase. The microsystem exhibits various motions including period-1,-2,-3, as well as chaotic. Furthermore, the bifurcation diagram of Poincaré sections includes 6 distinct highly chaotic regions. A further increase in F_1 makes the microsystem-motion periodic first, then at F_1=34.1, the microscale microtube starts to experience a period-2 motion until F_1=35.5. After this point, various motion types including period-3, period-4 and quasiperiodic motions occur before F_1=35.9, where the second chaos occurs. By further increasing F_1, some complex motions including other chaotic motions occur one after another. It should be noted that between the second and third chaotic motions, the microsystem undergoes a period-3 motion. Also, there is a period-2 motion proceeding with a period-4 one between the fourth and fifth chaotic motions, as shown in Fig. 4. For detail comparison purposes, the details of the motion at F_1=15 and F_1=44.9 are plotted in Figs. 5 and

6, respectively. As seen at F_1=15, the motion of the viscoelastic fluid-conveying microscale system is periodic while the system motion chaos at F_1=44.9.

Figure 7 depicts the bifurcation curves of viscoelastic microtubes containing flowing fluid with non-dimensional speed u_f=8.2; the microsystem is in the supercritical regime. It is observed that the microscale system experiences various types of complex dynamics such as period-1,-2,-5 as well as chaotic motion with increasing F_1 from 0 to 60; some details of the period-5 motion of the microsystem at F_1=11 is depicted in Fig. 8. For comparison purposes, the bifurcation curves of Poincaré sections of fluid-conveying viscoelastic microtubes for u_f=8.3 is also plotted in Fig. 9. From Figs. 8 and 9, it is found that the value of fluid velocity (even small increments sometimes) has a significant role to play in the dynamic behaviour of the viscoelastic microsystem. A small increase in the velocity of the flowing fluid results in a dramatic change in the bifurcation response of the microsystem. The complexity of the dynamic behaviour decreases with increasing the non-dimensional fluid velocity from 8.2 to 8.3. In other words, the number of chaotic regions decreases with increasing the speed of the flowing fluid after the critical point corresponding to divergence. Figure 10 shows some details of the microsystem motion described in Fig. 9 including the time histories and the phase-plane portrait of q_1 and q_2 as well as their FFTs at F_1=2.7. From the figure, a highly chaotic type of motion is clearly observed for the microscale tube.

4. Conclusions

In this paper, the nonlinear viscoelastically coupled behaviours of fluid-conveying microscale tubes subject to an external excitation force have been explored in details. The viscoelastic microtube was assumed to be resting on a nonlinear elastic foundation. In order to incorporate the effects of size dependency and viscoelastic characteristics, the MCS theory and Kelvin-Voigt model were employed, respectively. The continuous and discretised versions of the viscoelastic microsystem model were presented briefly. The resulting time-dependent coupled equations were finally solved within the framework of a time-integration scheme.

It was found that the velocity of the flowing fluid plays a crucial role in the complex motion of gyroscopic viscoelastic microscale pipes embedded in an elastic medium. By choosing a fluid velocity in the lower ranges of the subcritical regime, a complex chaotic motion can be avoided. When the speed of the flowing fluid approaches the critical velocity by growing values, the width of the period-1 region of the microsystem decreases substantially. However, both diversity and complexity of dynamic behaviour increase noticeably. Beyond the critical fluid velocity, the microsystem dynamics experiences a variety of complex motions such as period-1, -2, -5 and chaotic depending on the value of the external excitation load. In addition, it was observed that beyond the critical state corresponding to divergence, the number of chaotic regions decreases for larger flow velocities.

References

[1] R. Basutkar, Analytical modelling of a nanoscale series-connected bimorph piezoelectric energy harvester incorporating the flexoelectric effect, International Journal of Engineering Science, 139 (2019) 42-61.

[2] M.H. Jalaei, Ö. Civalek, On dynamic instability of magnetically embedded viscoelastic porous FG nanobeam, International Journal of Engineering Science, 143 (2019) 14-32.

[3] N. Shafiei, G.-L. She, On vibration of functionally graded nano-tubes in the thermal environment, International Journal of Engineering Science, 133 (2018) 84-98.

[4] D. Alveringh, R.J. Wiegerink, J.C. Lötters, Integrated pressure sensing using capacitive coriolis mass flow sensors, Journal of Microelectromechanical Systems, 26 (2017) 653-661.

[5] M.E. Warkiani, G. Guan, K.B. Luan, W.C. Lee, A.A.S. Bhagat, P.K. Chaudhuri, D.S.-W. Tan, W.T. Lim, S.C. Lee, P.C. Chen, Slanted spiral microfluidics for the ultra-fast, label-free isolation of circulating tumor cells, Lab on a Chip, 14 (2014) 128-137.

[6] M.H. Jalaei, A.G. Arani, H. Tourang, On the dynamic stability of viscoelastic graphene sheets, International Journal of Engineering Science, 132 (2018) 16-29.

[7] L. Lu, X. Guo, J. Zhao, On the mechanics of Kirchhoff and Mindlin plates incorporating surface energy, International Journal of Engineering Science, 124 (2018) 24-40.

[8] T. Natsuki, J. Natsuki, Transverse impact analysis of double-layered graphene sheets on an elastic foundation, International Journal of Engineering Science, 124 (2018) 41-48.

[9] H. Shahverdi, M.R. Barati, Vibration analysis of porous functionally graded nanoplates, International Journal of Engineering Science, 120 (2017) 82-99.

[10] R. Barretta, S.A. Faghidian, F. Marotti de Sciarra, Stress-driven nonlocal integral elasticity for axisymmetric nano-plates, International Journal of Engineering Science, 136 (2019) 38-52.

[11] M.A. Attia, A.A. Abdel Rahman, On vibrations of functionally graded viscoelastic nanobeams with surface effects, International Journal of Engineering Science, 127 (2018) 1-32.

[12] R. Barretta, M. Čanađija, R. Luciano, F.M. de Sciarra, Stress-driven modeling of nonlocal thermoelastic behavior of nanobeams, International Journal of Engineering Science, 126 (2018) 53-67.

[13] B. Karami, M. Janghorban, On the dynamics of porous nanotubes with variable material properties and variable thickness, International Journal of Engineering Science, 136 (2019) 53-66.

[14] H.B. Khaniki, On vibrations of nanobeam systems, International Journal of Engineering Science, 124 (2018) 85-103.

[15] L. Li, H. Tang, Y. Hu, The effect of thickness on the mechanics of nanobeams, International Journal of Engineering Science, 123 (2018) 81-91.

[16] H.B. Khaniki, On vibrations of FG nanobeams, International Journal of Engineering Science, 135 (2019) 23-36.

[17] G.-L. She, Y.-R. Ren, F.-G. Yuan, W.-S. Xiao, On vibrations of porous nanotubes, International Journal of Engineering Science, 125 (2018) 23-35.

[18] A.M. Dehrouyeh-Semnani, M. Nikkhah-Bahrami, M.R.H. Yazdi, On nonlinear vibrations of micropipes conveying fluid, International Journal of Engineering Science, 117 (2017) 20-33.

[19] H. Farokhi, M.H. Ghayesh, A. Gholipour, Dynamics of functionally graded micro-cantilevers, International Journal of Engineering Science, 115 (2017) 117-130.

[20] Ç. Demir, Ö. Civalek, On the analysis of microbeams, International Journal of Engineering Science, 121 (2017) 14-33.

[21] H. Farokhi, M.H. Ghayesh, A. Gholipour, S. Hussain, Motion characteristics of bilayered extensible Timoshenko microbeams, International Journal of Engineering Science, 112 (2017) 1-17.

[22] M.H. Ghayesh, H. Farokhi, A. Gholipour, S. Hussain, On the nonlinear mechanics of layered microcantilevers, International Journal of Engineering Science, 120 (2017) 1-14.

[23] A. Pourasghar, Z. Chen, Effect of hyperbolic heat conduction on the linear and nonlinear vibration of CNT reinforced size-dependent functionally graded microbeams, International Journal of Engineering Science, 137 (2019) 57-72.

[24] L. Qi, S. Huang, G. Fu, S. Zhou, X. Jiang, On the mechanics of curved flexoelectric microbeams, International Journal of Engineering Science, 124 (2018) 1-15.

[25] H. Farokhi, M.H. Ghayesh, On the dynamics of imperfect shear deformable microplates, International Journal of Engineering Science, 133 (2018) 264-283.

[26] M. Rahaeifard, M. Mojahedi, On the mechanics of laminated microplates, International Journal of Engineering Science, 119 (2017) 180-188.

[27] M.H. Ghayesh, H. Farokhi, A. Gholipour, M. Tavallaeinejad, Nonlinear oscillations of functionally graded microplates, International Journal of Engineering Science, 122 (2018) 56-72.

[28] H. Farokhi, M.H. Ghayesh, Nonlinear mechanics of electrically actuated microplates, International Journal of Engineering Science, 123 (2018) 197-213.

[29] R. Bahaadini, A.R. Saidi, M. Hosseini, On dynamics of nanotubes conveying nanoflow, International Journal of Engineering Science, 123 (2018) 181-196.

[30] F. Ebrahimi, M.R. Barati, A nonlocal higher-order refined magneto-electro-viscoelastic beam model for dynamic analysis of smart nanostructures, International Journal of Engineering Science, 107 (2016) 183-196.

[31] N.M. Faleh, R.A. Ahmed, R.M. Fenjan, On vibrations of porous FG nanoshells, International Journal of Engineering Science, 133 (2018) 1-14.

[32] A. Hadi, M.Z. Nejad, M. Hosseini, Vibrations of three-dimensionally graded nanobeams, International Journal of Engineering Science, 128 (2018) 12-23.

[33] L. Lu, X. Guo, J. Zhao, A unified nonlocal strain gradient model for nanobeams and the importance of higher order terms, International Journal of Engineering Science, 119 (2017) 265-277.

[34] X. Zhu, L. Li, On longitudinal dynamics of nanorods, International Journal of Engineering Science, 120 (2017) 129-145.

[35] F. Ebrahimi, M.R. Barati, A. Dabbagh, A nonlocal strain gradient theory for wave propagation analysis in temperature-dependent inhomogeneous nanoplates, International Journal of Engineering Science, 107 (2016) 169-182.

[36] L. Lu, X. Guo, J. Zhao, Size-dependent vibration analysis of nanobeams based on the nonlocal strain gradient theory, International Journal of Engineering Science, 116 (2017) 12-24.

[37] M. Şimşek, Nonlinear free vibration of a functionally graded nanobeam using nonlocal strain gradient theory and a novel Hamiltonian approach, International Journal of Engineering Science, 105 (2016) 12-27.

[38] X. Zhu, L. Li, Closed form solution for a nonlocal strain gradient rod in tension, International Journal of Engineering Science, 119 (2017) 16-28.

[39] S.A. Faghidian, Integro-differential nonlocal theory of elasticity, International Journal of Engineering Science, 129 (2018) 96-110.

[40] J. Fernández-Sáez, R. Zaera, Vibrations of Bernoulli-Euler beams using the two-phase nonlocal elasticity theory, International Journal of Engineering Science, 119 (2017) 232-248.

[41] G. Romano, R. Barretta, Nonlocal elasticity in nanobeams: the stress-driven integral model, International Journal of Engineering Science, 115 (2017) 14-27.

[42] A. Apuzzo, R. Barretta, S.A. Faghidian, R. Luciano, F. Marotti de Sciarra, Free vibrations of elastic beams by modified nonlocal strain gradient theory, International Journal of Engineering Science, 133 (2018) 99-108.

[43] M.H. Ghayesh, A. Farajpour, Nonlinear mechanics of nanoscale tubes via nonlocal strain gradient theory, International Journal of Engineering Science, 129 (2018) 84-95.

[44] M.H. Ghayesh, A. Farajpour, A review on the mechanics of functionally graded nanoscale and microscale structures, International Journal of Engineering Science, 137 (2019) 8-36.

[45] L.-L. Ke, C. Liu, Y.-S. Wang, Free vibration of nonlocal piezoelectric nanoplates under various boundary conditions, Physica E: Low-dimensional Systems and Nanostructures, 66 (2015) 93-106.

[46] H. Farokhi, M.H. Ghayesh, Nonlinear dynamical behaviour of geometrically imperfect microplates based on modified couple stress theory, International Journal of Mechanical Sciences, 90 (2015) 133-144.

[47] M. Şimşek, Dynamic analysis of an embedded microbeam carrying a moving microparticle based on the modified couple stress theory, International Journal of Engineering Science, 48 (2010) 1721-1732.

[48] Y. Sugiyama, Y. Tanaka, T. Kishi, H. Kawagoe, Effect of a spring support on the stability of pipes conveying fluid, Journal of Sound and Vibration, 100 (1985) 257-270.

[49] M.H. Ghayesh, M.P. Païdoussis, Y. Modarres-Sadeghi, Three-dimensional dynamics of a fluid-conveying cantilevered pipe fitted with an additional spring-support and an end-mass, Journal of Sound and Vibration, 330 (2011) 2869-2899.

[50] L. Wang, Size-dependent vibration characteristics of fluid-conveying microtubes, Journal of Fluids and Structures, 26 (2010) 675-684.
[51] S. Kural, E. Özkaya, Size-dependent vibrations of a micro beam conveying fluid and resting on an elastic foundation, Journal of Vibration and Control, 23 (2017) 1106-1114.
[52] A.M. Dehrouyeh-Semnani, H. Zafari-Koloukhi, E. Dehdashti, M. Nikkhah-Bahrami, A parametric study on nonlinear flow-induced dynamics of a fluid-conveying cantilevered pipe in post-flutter region from macro to micro scale, International Journal of Non-Linear Mechanics, 85 (2016) 207-225.
[53] M. Hosseini, R. Bahaadini, Size dependent stability analysis of cantilever micro-pipes conveying fluid based on modified strain gradient theory, International Journal of Engineering Science, 101 (2016) 1-13.
[54] M. Mohammadimehr, M. Mehrabi, Stability and free vibration analyses of double-bonded micro composite sandwich cylindrical shells conveying fluid flow, Applied Mathematical Modelling, 47 (2017) 685-709.

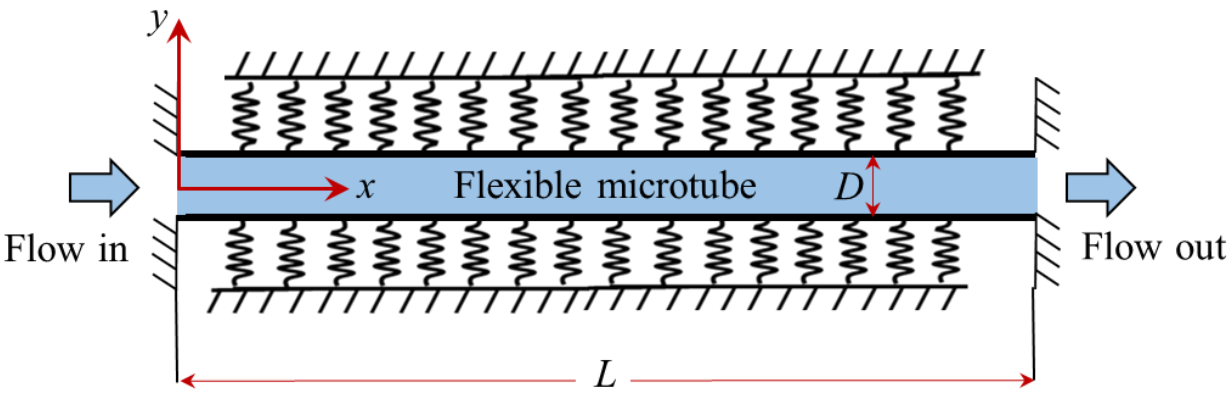

Figure 1: A microscale flexible fluid-conveying viscoelastic microtube embedded in a nonlinear elastic medium.

(a)

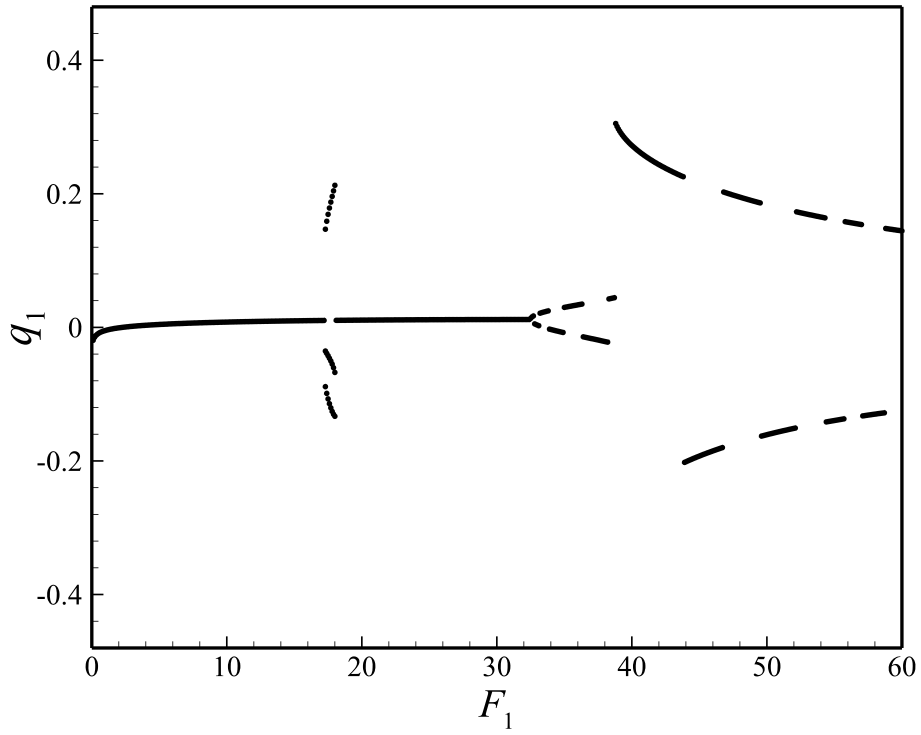
0.4
0.2
0
-0.2
-0.4
q_1
0
10
20
30
40
50
60
F_1

(b)

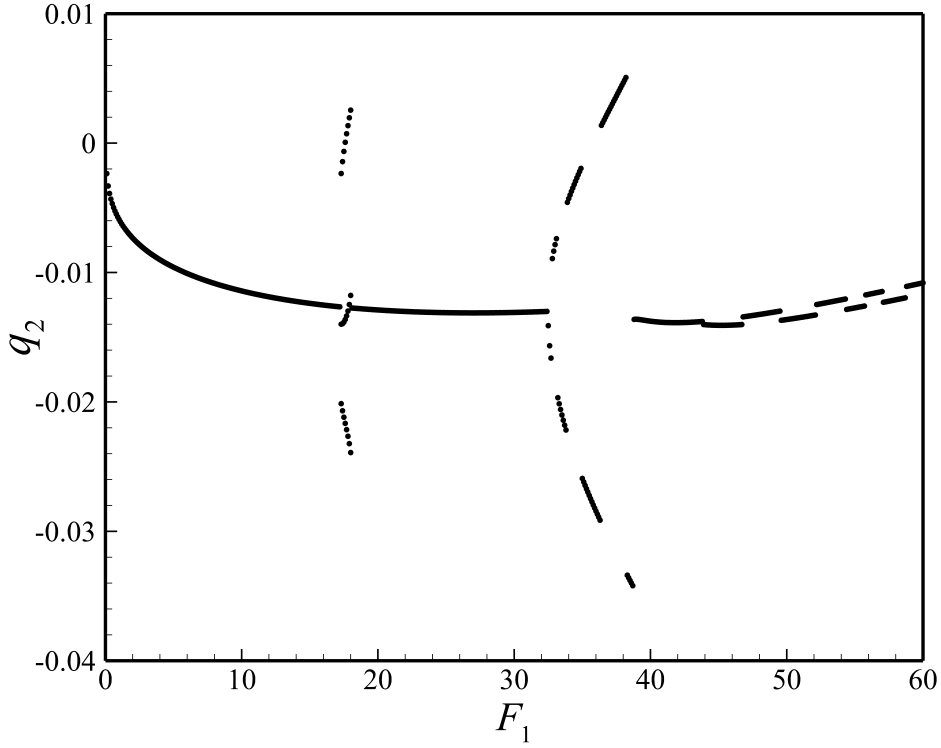
0.01
0
-0.01
-0.02
-0.03
-0.04
q_2
0
10
20
30
40
50
60
F_1

(c)

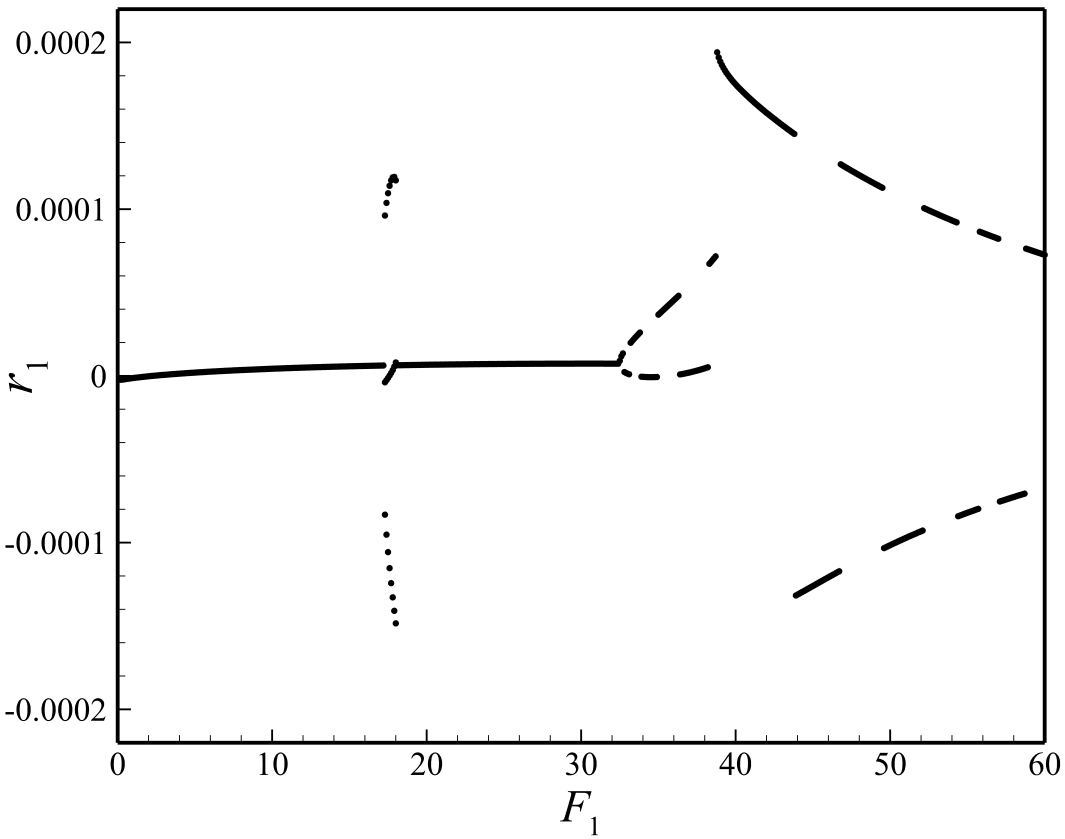

Figure 2: Bifurcation curves of Poincaré sections for fluid-conveying viscoelastic microtubes for u_f=7.9.

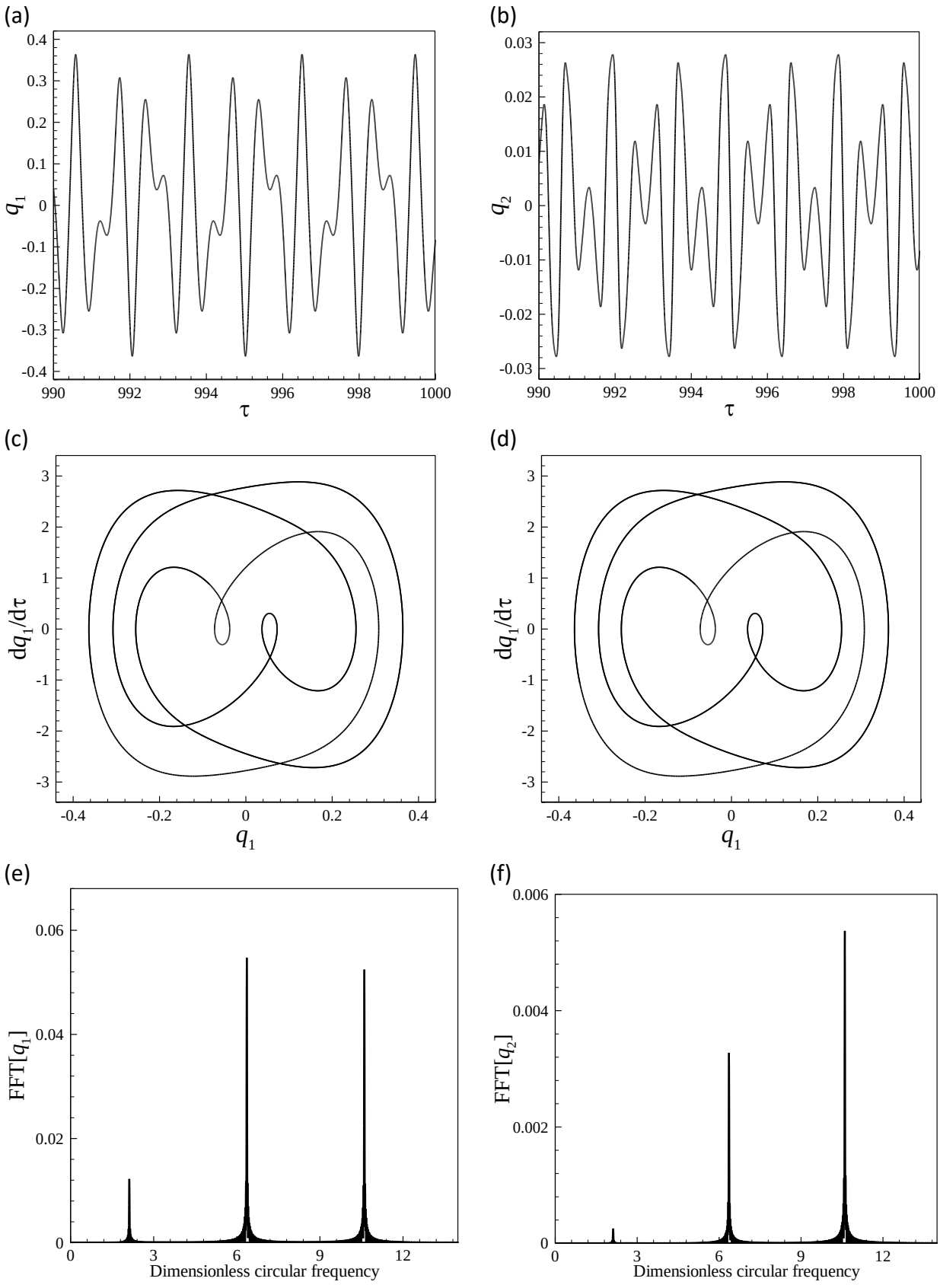
(a)
(b)
(c)
(d)
(e)
(f)
q_1
q_2
τ
$dq_1/d\tau$
q_1
FFT[q_1]
FFT[q_2]
Dimensionless circular frequency
Dimensionless circular frequency

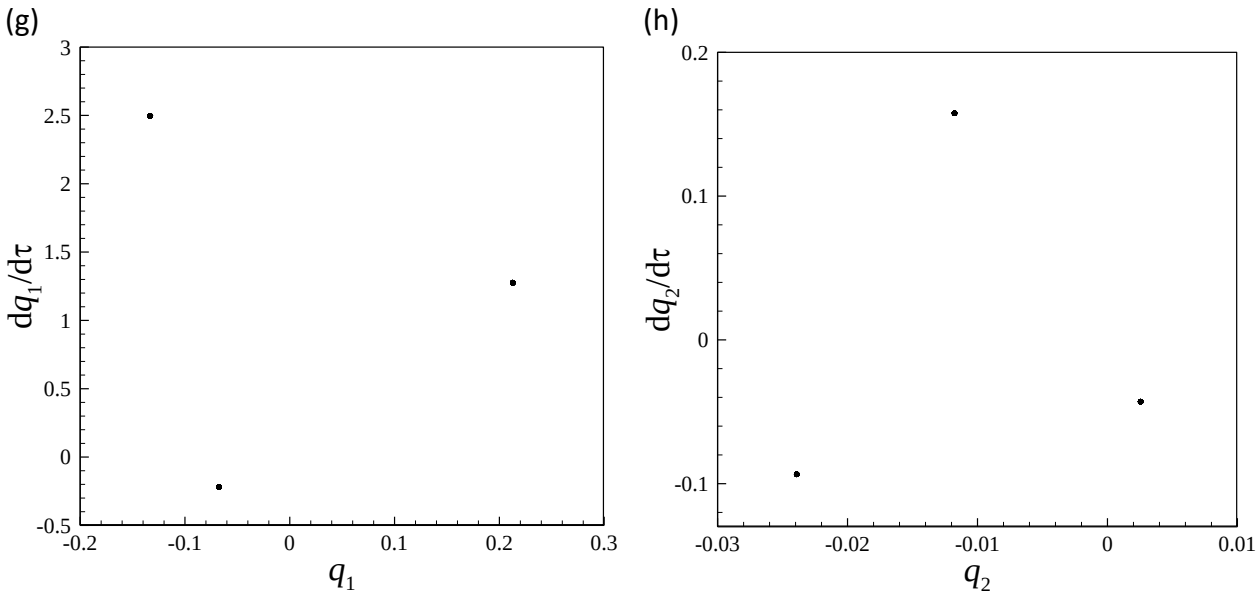

Figure 3: Period-3 motion observed in Fig. 2 for F_1=18.0.

(a)

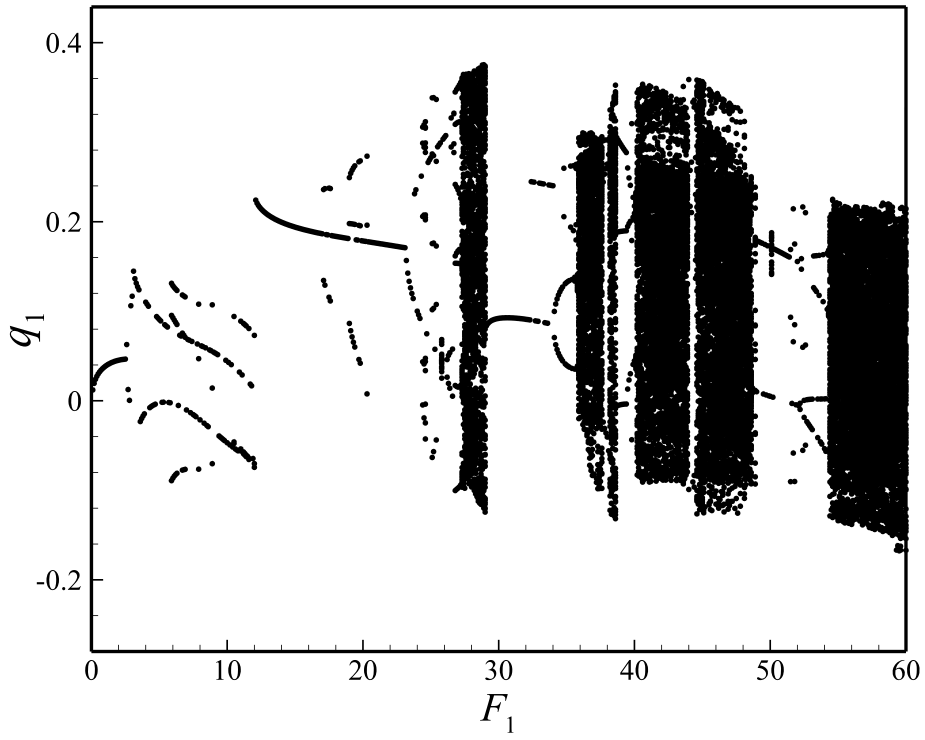
0.4
0.2
0
-0.2
q_1
0
10
20
30
40
50
60
F_1

(b)

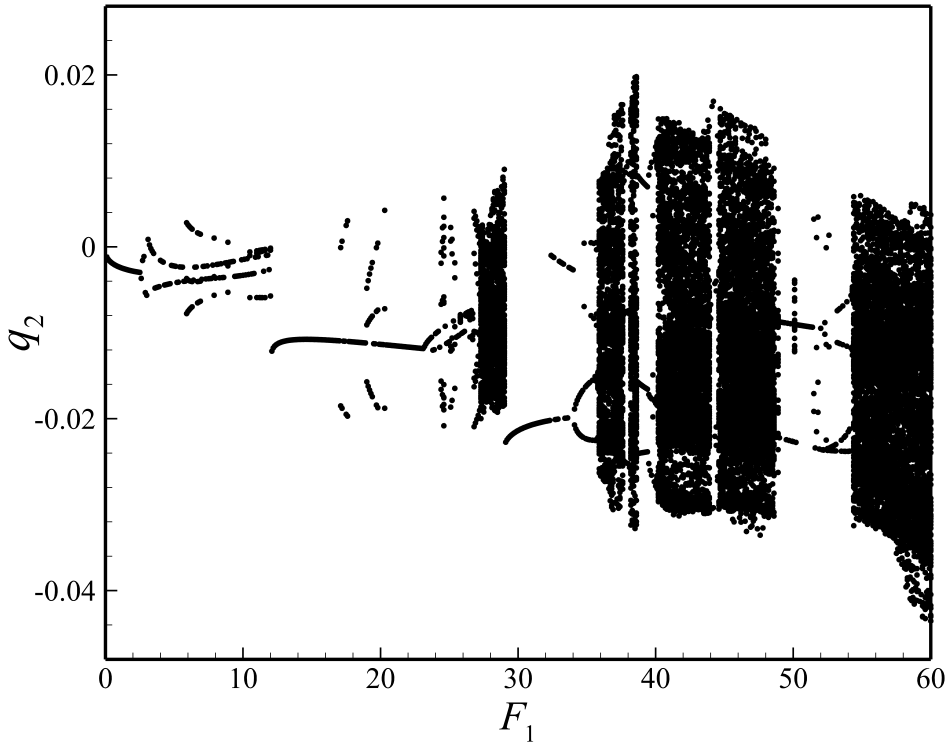
0.02
0
-0.02
-0.04
q_2
0
10
20
30
40
50
60
F_1

(c)

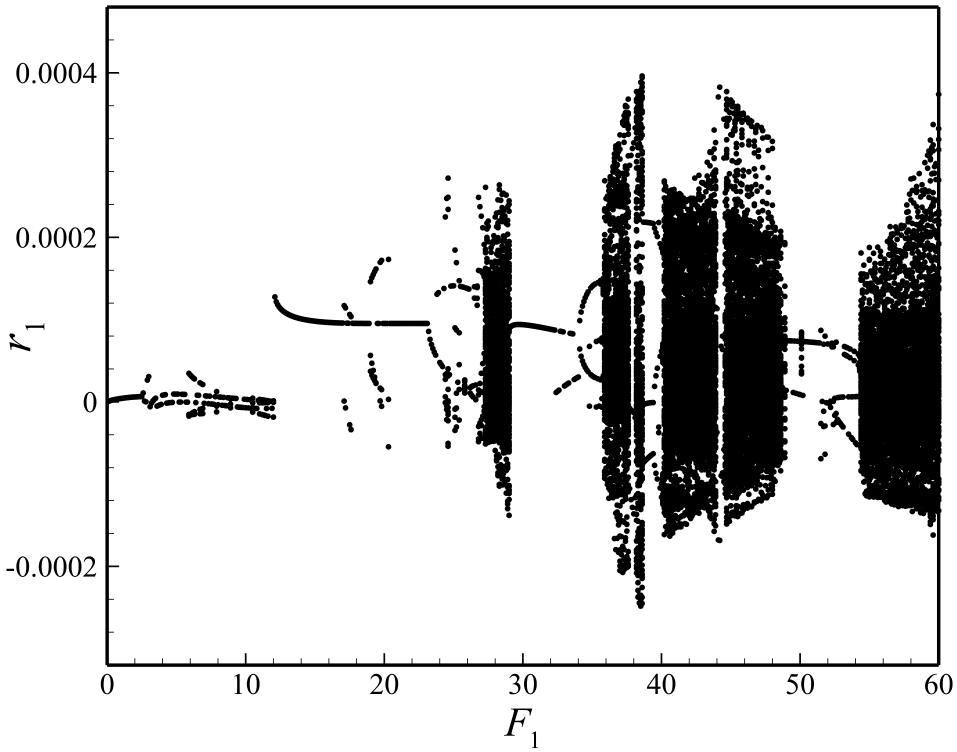

Figure 4: Bifurcation curves of Poincaré sections for fluid-conveying viscoelastic microtubes for u_f = 8.1.

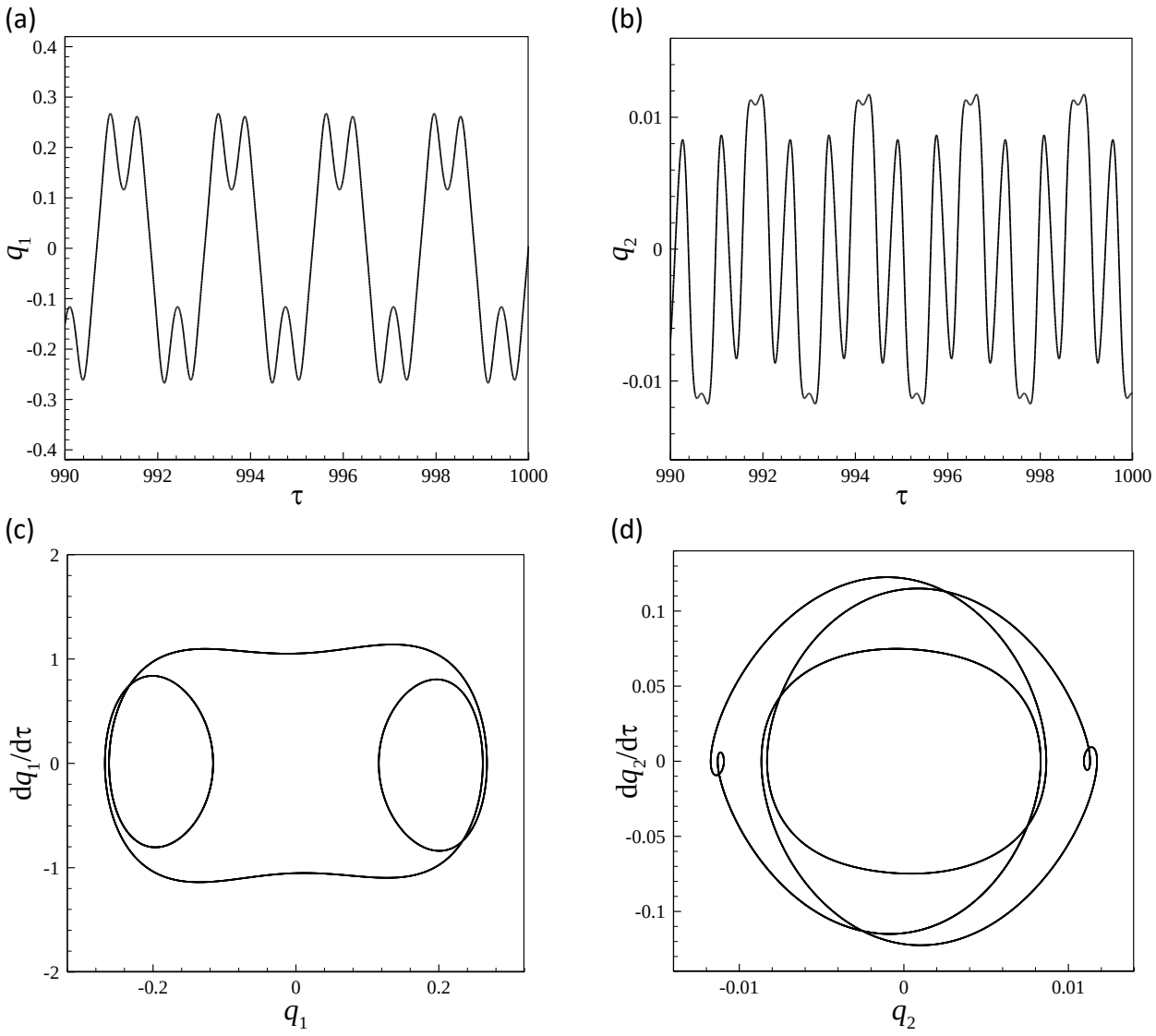

Figure 5: Period-1 motion observed in Fig. 4 for F_1=15.0.

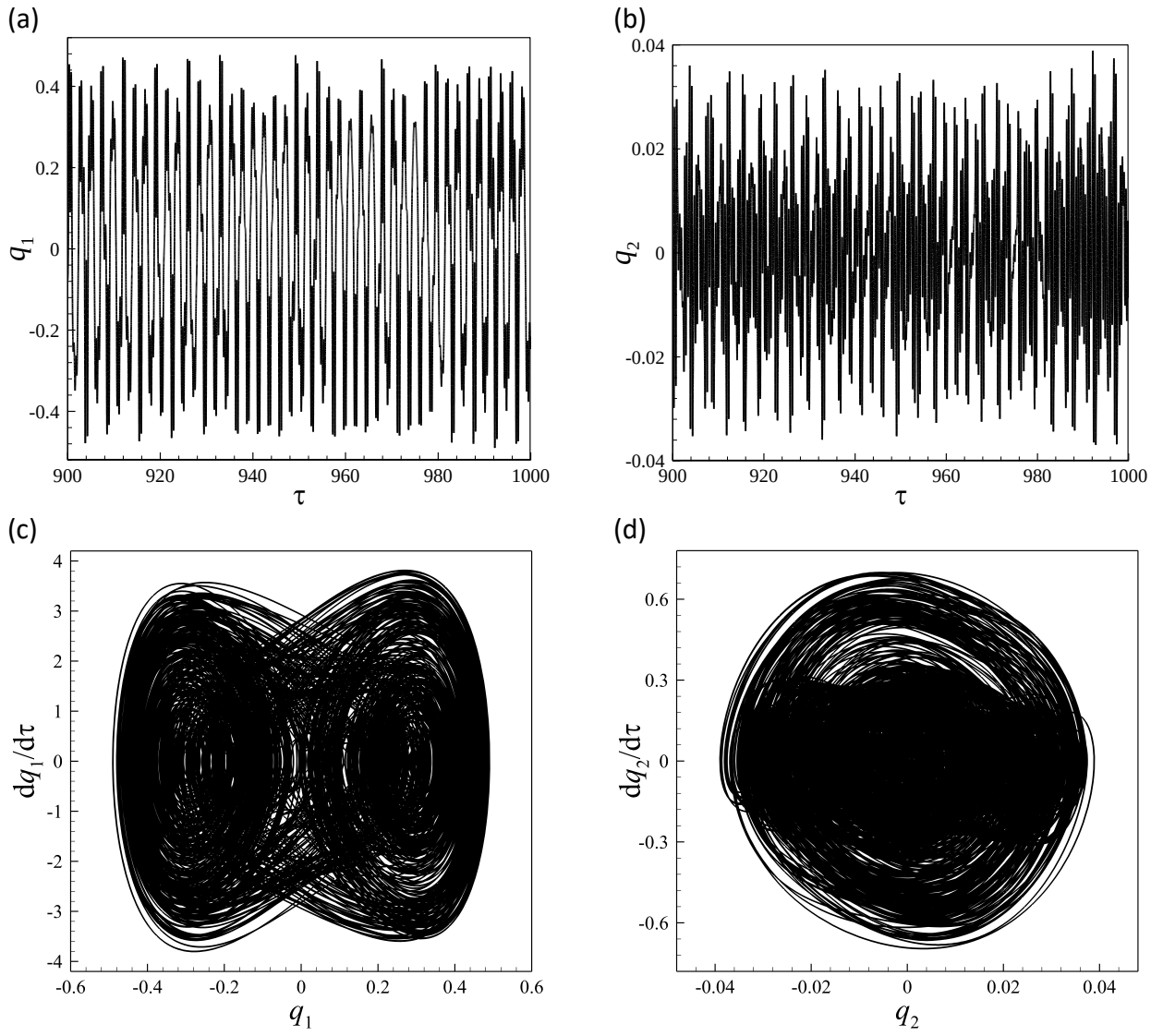

Figure 6: Chaotic motion observed in Fig. 4 for F_1=44.9.

(a)

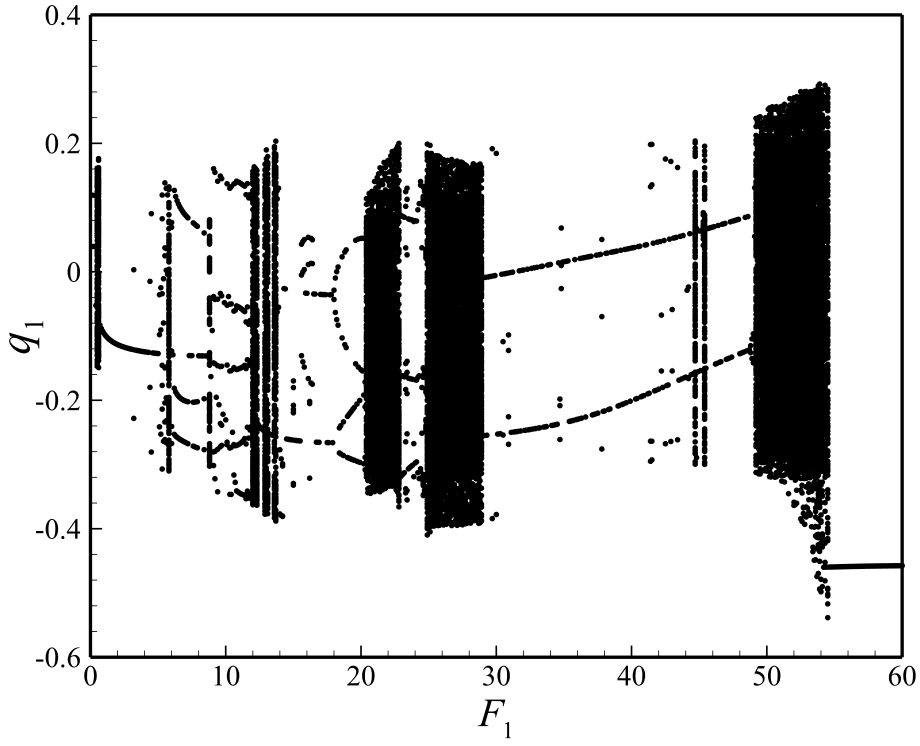
0.4
0.2
0
-0.2
-0.4
-0.6
q_1
0
10
20
30
40
50
60
F_1

(b)

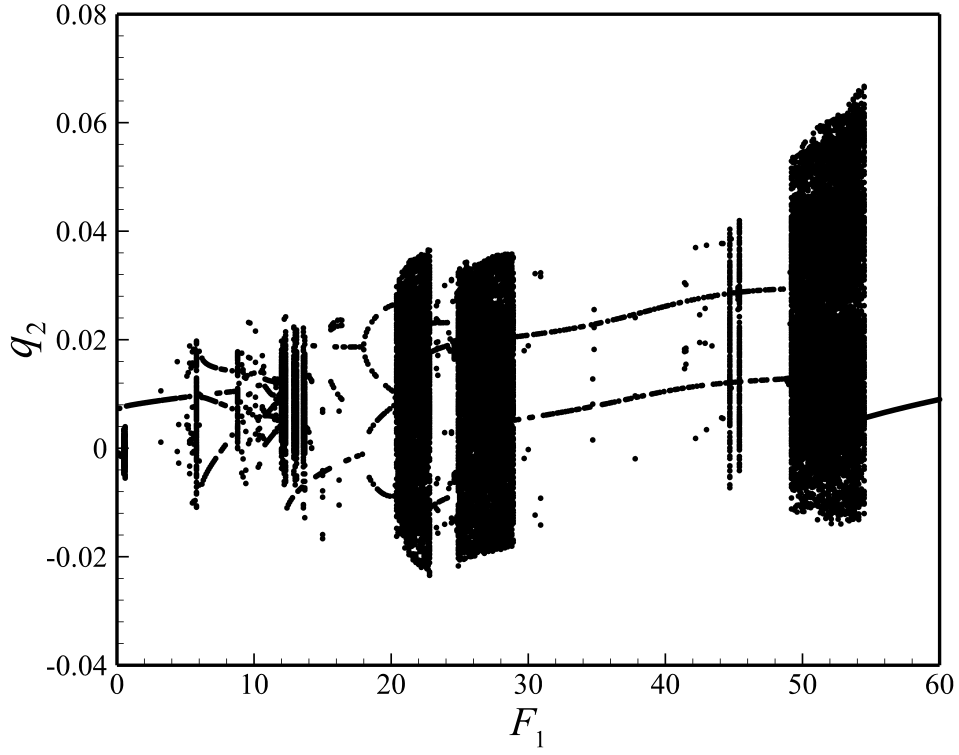
0.08
0.06
0.04
0.02
0
-0.02
-0.04
q_2
0
10
20
30
40
50
60
F_1

(c)

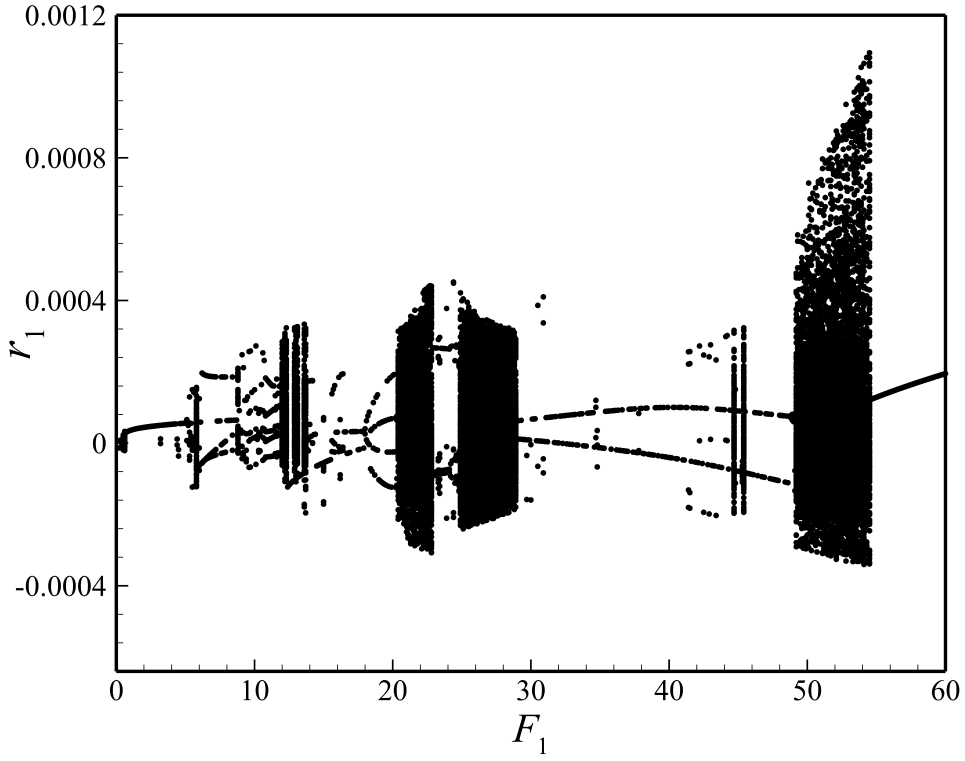

Figure 7: Bifurcation curves of Poincaré sections for fluid-conveying viscoelastic microtubes for u_f = 8.2.

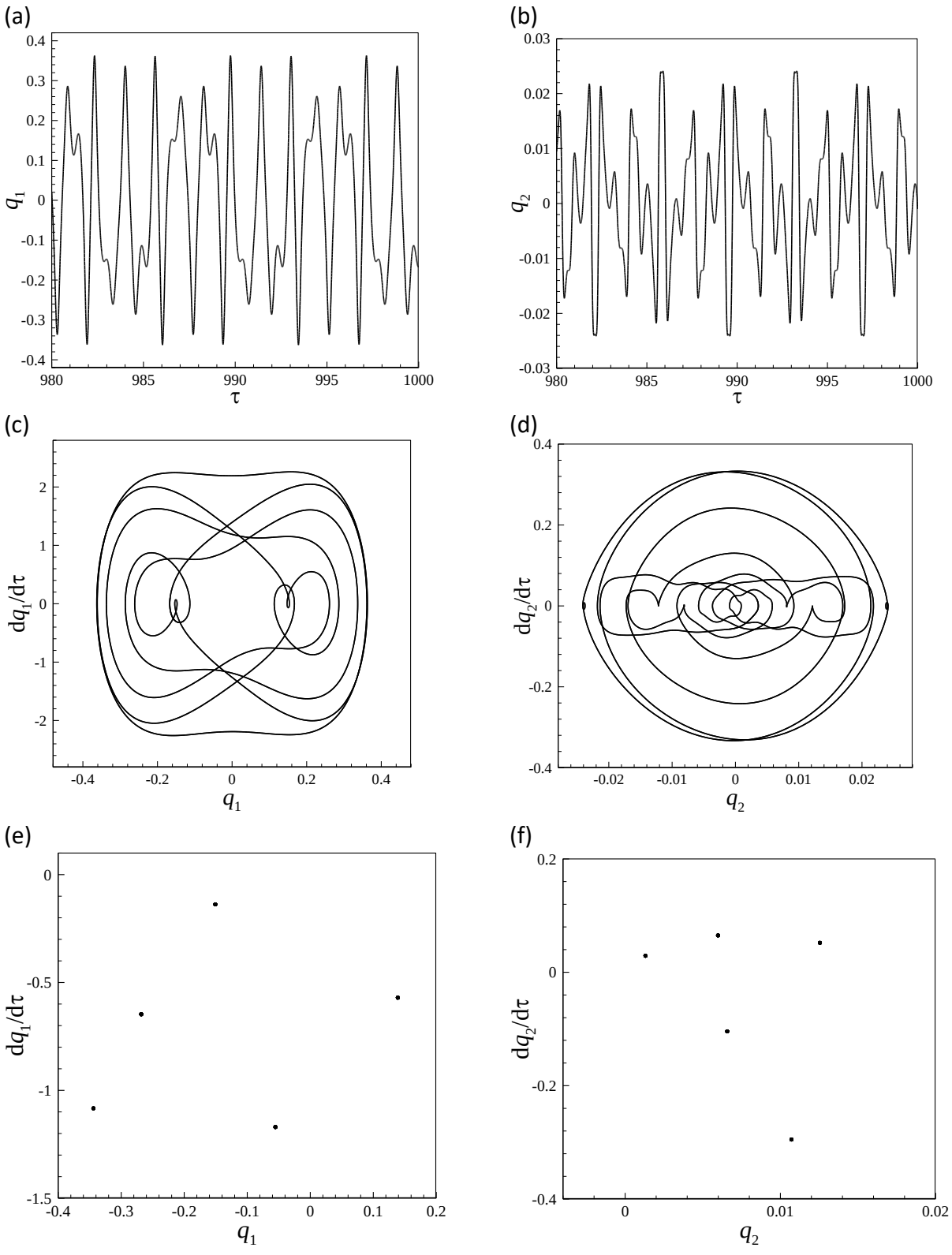

Figure 8: Period-5 motion observed in Fig. 7 for F_1=11.0.

(a)

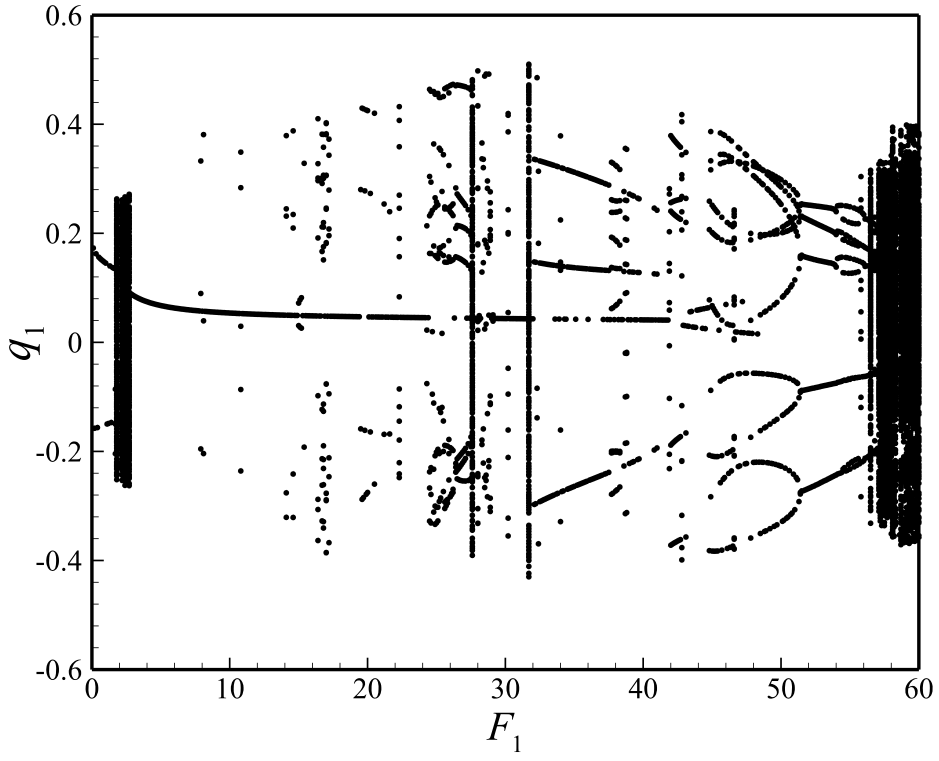
0.6
0.4
0.2
0
-0.2
-0.4
-0.6
q_1
0
10
20
30
40
50
60
F_1

(b)

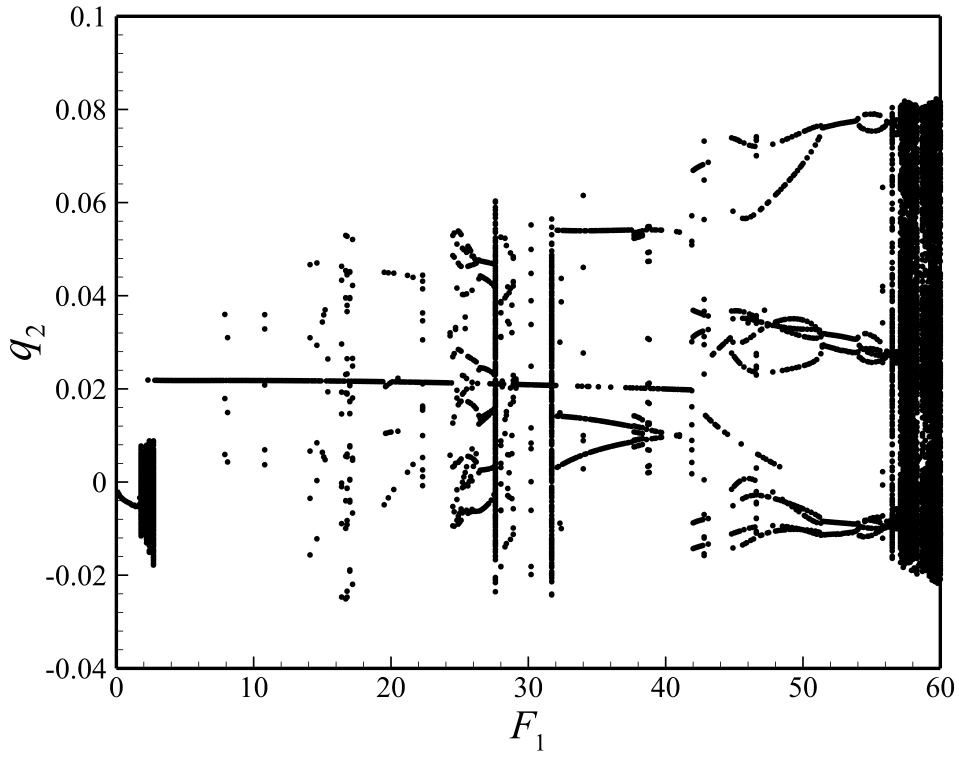
0.1
0.08
0.06
0.04
0.02
0
-0.02
-0.04
q_2
0
10
20
30
40
50
60
F_1

(c)

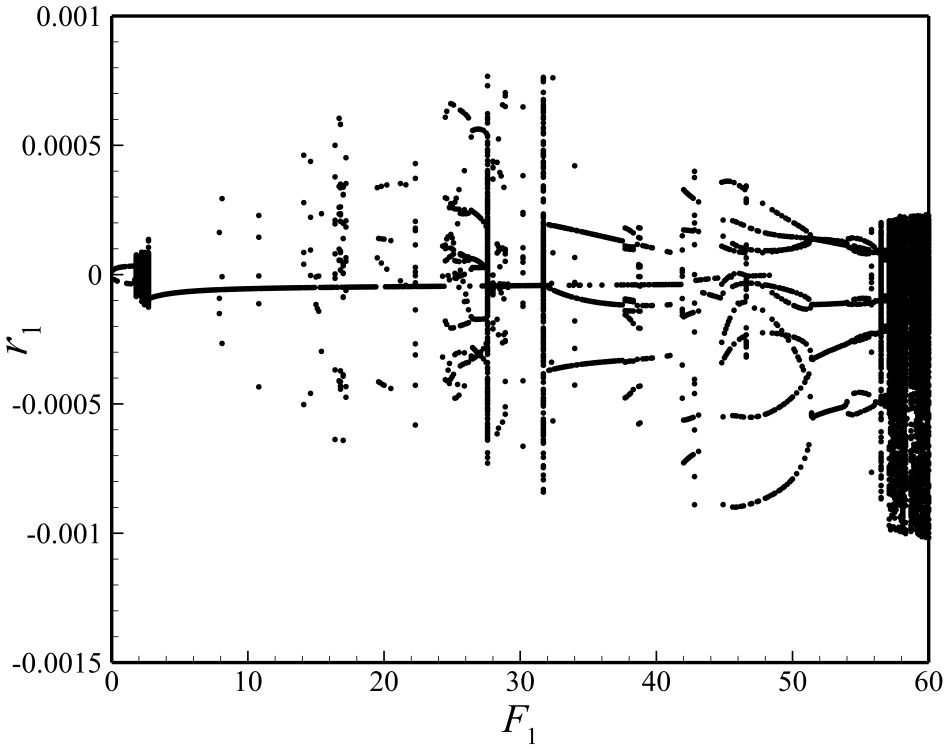

Figure 9: Bifurcation plots of Poincaré sections for fluid-conveying viscoelastic microtubes for u_f = 8.3.

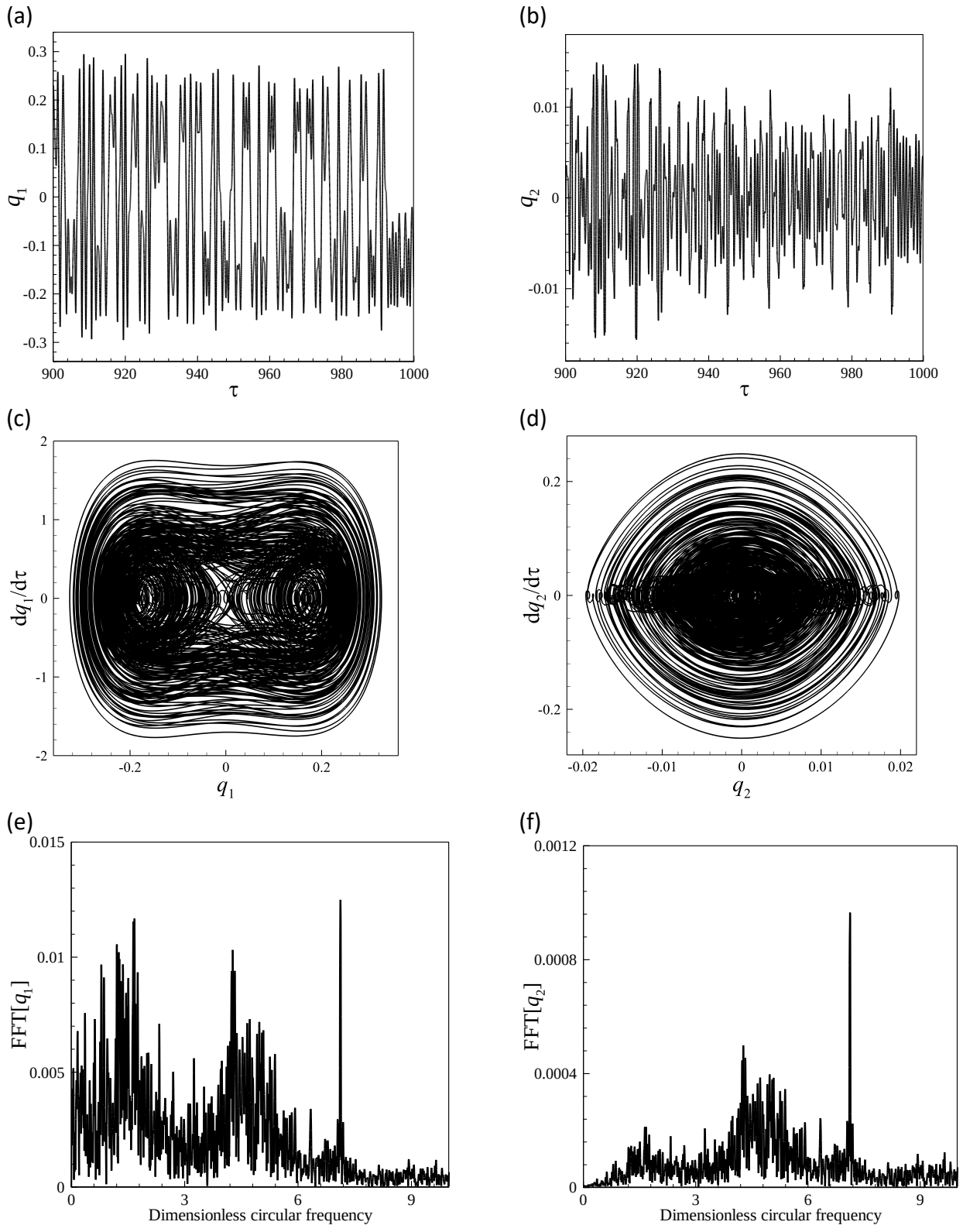

Figure 10: Chaotic motion observed in Fig. 9 for F_1=2.7.